Distinct T cell chromatin landscapes in scleroderma subtypes

Diana R. Dou[1], Yang Zhao[1], Brian Abe[1,3], Rui Li[1], Lisa C. Zaba[1,2], Kathleen Aren[4], Mary Carns [4], Lorinda S. Chung[3], Monique Hinchcliff[4,5,6], Howard Y. Chang[1,2,6]

[1] Center for Personal Dynamic Regulomes, Stanford University, Stanford, CA, USA.
[2] Department of Dermatology, Stanford University School of Medicine, Stanford, CA, USA.
[3] Division of Immunology and Rheumatology, Stanford University School of Medicine, Stanford, CA, USA.
[4] Northwestern University Feinberg School of Medicine, Department of Medicine, Division of Rheumatology, Chicago, IL, USA.
[5] Section of Allergy, Rheumatology & Immunology, Yale School of Medicine, New Haven, Connecticut, USA.
[6] Co-senior authors

Correspondence to: howchang@stanford.edu and monique.hinchcliff@yale.edu

ABSTRACT

Systemic sclerosis (SSc; scleroderma) is an autoimmune rheumatic disease that primarily affects biological females whose pathogenesis is poorly understood. The clinical hallmark is hardening of the skin, but internal organ dysfunction is the leading cause of death. Diagnosis and treatment are complicated by heterogeneity within the disease including variable lethality, fibrosis severity, serum autoantibody production, and internal organ involvement. Important gaps remain in our knowledge of the exact molecular and cellular pathways underlying distinct SSc subtypes. Herein, we identify genome-wide chromatin accessibility profiles of peripheral $CD4^+$ T cells to distinguish and better understand the observed heterogeneity in SSc patients. We identify a link between the presence of serum anticentromere autoantibodies (ACA) and elevated levels of T helper 2 (Th2) cells and increased chromatin access at gene loci encoding fibrosis-driving Th2 cytokines IL4, IL13, and IL4 receptor. Biological sex followed by autoantibody type are the predominant variables associated with differences in $CD4^+$ T cell epigenomic profiles, while mycophenolate mofetil treatment appeared to have no effect. These results suggest new mechanistic basis and therapeutic strategies to address SSc, especially the anti-ACA+ subset of patients who more frequently develop pulmonary arterial hypertension.

INTRODUCTION

Systemic sclerosis (SSc; scleroderma) is a clinically heterogeneous systemic disease with the highest case-fatality rate of autoimmune rheumatic diseases (Hinchcliff et al., 2021). Although disease pathogenesis was thought to involve an early vascular phase followed by immune dysregulation and skin and internal organ fibrosis, it is more likely that the three pathological processes develop concurrently (Gjeloshi et al., 2020). In spite of these insights, a poor understanding of the deregulated molecular systems that drive SSc remains. Two clinical SSc subtypes, limited cutaneous (lc) and diffuse cutaneous (dc) have been described based upon

the pattern and extent of skin fibrosis (LeRoy et al., 1988). The role of serum autoantibodies as more than diagnostic indicators of autoimmune disease has increasingly come to light (Domsic and Medsger, 2016). In particular, anti-RNA polymerase III (RNAIII) autoantibodies are associated with an increased risk for scleroderma renal crisis and worse skin fibrosis while anticentromere antibodies (ACA) are associated with the development of pulmonary arterial hypertension (PAH) (Domsic and Medsger, 2016), but many gaps persist between autoantibody profiles and clinical disease manifestations.

Immune modulators, such as mycophenolate mofetil (MMF) that inhibits purine synthesis and reduces lymphocyte proliferation, are often prescribed for SSc lung and skin disease (Hinchcliff et al., 2013; Walker et al., 2012), yet response is variable (Herrick et al., 2010; Panopoulos et al., 2013). Study results suggest that innate immune system activation plays a critical role in SSc pathogenesis (Chia and Lu, 2015; Christmann et al., 2011; Christmann et al., 2014; Guilpain et al., 2021; Higashi-Kuwata et al., 2010; Johnson et al., 2015; Skaug et al., 2020). Perivascular lymphocytes are a predominant feature of early SSc skin disease and many therapies used in treating other skin and autoimmune diseases, such as B-cell depletion with rituximab, and cyclophosphamide (also acts on T-cells), MMF (also acts on T-cells), tocilizumab and abatacept have also been utilized in the treatment of SSc skin disease with varied success (Daoussis et al., 2012; Fernández-Codina et al., 2018; Jordan et al., 2015; Khanna et al., 2020; Taroni et al., 2017). Drugs targeting T-cells, specifically IL-4 and -13, including romilkumab and dupilumab are also under investigation (Allanore et al., 2020a; Gasparini et al., 2020). To date, no drugs have been identified that are uniformly useful in the treatment of SSc skin fibrosis. Thus, a better understanding of the molecular derangements that underlie SSc skin disease are required to permit identification of targeted effective therapy.

The majority of existing genomic profiling in SSc patients has focused on differential gene expression, but the role of chromatin accessibility contributes greatly to gene regulation in health and disease and is an important noncoding metric for cell and tissue identity and functionality. Assay for Transposase-Accessible Chromatin by sequencing (ATAC-seq) is capable of interrogating the chromatin landscape at high sensitivity in rare cell types and particularly optimized in blood cells (Buenrostro et al., 2013; Corces et al., 2016; Corces et al., 2017). Furthermore, ATAC-seq profiling of chromatin accessibility patterns in multiple human primary blood cell types reflected cell identity better than mRNA expression levels obtained through RNA-seq (Corces et al., 2016). ATAC-seq is, therefore, a powerful tool for assessing, with high sensitivity and accuracy, genomic profiles unique to SSc and its clinically-defined subsets.

Herein, we characterize genome-wide chromatin accessibility state of circulating $CD4^+$ lymphocytes from patients with active SSc skin disease prior to initiation of MMF and at regular intervals during treatment and determine associations with clinical variables of treatment, biological sex, age, and serum autoantibody expression.

RESULTS

Clinical characteristics are shown in **Table 1** and **Supplemental Table 1** for 18 subjects with SSc (14 of 18 patients, 77.8% with dcSSc). The median (range: 0.5-142.5 months) SSc disease duration between first Raynaud symptom and the initial visit was 16 (stdev of 42.6) months. The median (range: 2-43) modified Rodnan skin score (mRSS) was 13.5 (stdev of 10.6). 3 subjects

(16.7%) had anticentromere antibodies (ACA), 9 (50%) had anti-RNA polymerase III (RNAIII), and only 1 (5.6%) had anti-topoisomerase I/Scl-70 serum autoantibodies as identified using the clinical laboratory (Specialty Labs, Valencia, CA).

Longitudinal profiling of systemic sclerosis patients

Peripheral blood was collected through venipuncture from consenting patients followed by $CD4^+$ Rosette separation and FACS selection of $CD3^+CD4^+$ T-lymphocytes for ATAC library preparation (Corces et al., 2017) (**Figure 1A**). A total of 18 patients comprised of 14 females and 4 males (**Table 1)** were analyzed across three separate timepoints, henceforth referred to as timepoint 1 (or, *baseline* if treatment naïve or falling within two months of treatment start date), timepoint 2 and timepoint 3 (**Supplementary Table 1**). ATAC-seq library quality checks and mitochondrial SNP profiling—to confirm consistent identity of each patient across each timepoint—were performed prior to analyses (**Supplemental Table 1, Supplemental Figure 1**).

Variables considered included patient age at blood collection, sample timepoint, biological sex, SSc subtype (limited or diffuse cutaneous), skin disease over the study course (improved, stable, worsened), skin disease treatment (MMF or treatment naïve), presence of any of three SSc-specific serum autoantibodies (ACA, RNAIII, and/or Scl70), and specifically ACA and RNAIII autoantibody status (Scl70 was not studied due to low prevalence in the study cohort, n=1) (**Table 1, Figure 1B**). Because Principal Components Analysis (PCA) showed that ACA positivity individually had larger variation than the three SSc autoantibodies grouped together (i.e. SSc autoantibodies expressed vs. none) (**Figure 1B**), we focused our studies on the ACA and RNAIII antibodies individually.

PCA performed on all sample ATAC-seq data identified that sex followed by SSc autoantibody status (specifically ACA positivity) and, to a lesser extent, age and treatment was associated with the most data variance (**Figure 1B, Supplemental Figure 1E**). There was very little ATAC-seq peak overlap between the individual variables (**Figure 1C**), indicating that these differences are attributable to each variable. GWAS-enrichment analysis of ATAC-seq data demonstrated significant alignment to multiple autoimmune diseases including, as expected, SSc as well as other rheumatic diseases (i.e., rheumatoid arthritis) (**Figure 1D**). Furthermore, associated ontology from the GWAS SNPs enriched in our dataset highlighted autoimmune-related pathways and categories as well as SSc-specific disease-drivers, such as Th1/Th2 differentiation, IL-35 and IL-21 signaling, NFKB signaling, and IFN-alpha production (**Figure 1E**) (Dantas et al., 2015).

MMF treatment does not significantly alter $CD4^+$ T-cells in SSc peripheral blood

Mycophenolate mofetil (MMF) is a commonly used treatment for various autoimmune diseases that works through inhibiting lymphocyte proliferation to decrease elevated immune activity and fibrosis (Allison and Eugui, 2000; Hinchcliff et al., 2013; Taroni et al., 2017). In this study, patients with active skin disease in the opinion of one treating physician based upon physical exam findings (described in **Materials and Methods**) were prescribed MMF while a control group of patients with stable, non-active disease remained untreated. To determine the potential impact of MMF treatment on T helper cells in SSc, we identified patients who donated a blood sample within two months of treatment initiation (baseline) as well as at two subsequent

treatment timepoints. Using these criteria, we compared the $CD4^+$ T-cell ATAC-seq profile of eight MMF-treated, and four untreated, patients (**Supplemental Table 1**).

Comparison of all peaks over the three timepoints showed a stable, unchanging pattern in MMF-treated patients and very few changes in untreated patients (**Figure 2A, 2C**). Similarly, CIBERSORT analysis using ATAC-seq data showed that the relative proportions of T-cell subsets within the $CD4^+$ population are also not significantly impacted by MMF treatment or lack of treatment (**Figure 2D, Supplemental Figure 2**). The differential peaks identified between the MMF-treated and untreated groups at baseline (**Figure 1C**) remain consistent at subsequent timepoints and thus may be explained by differences in SSc disease severity and activity at study onset (**Figure 2B**). Based on these results, MMF treatment in SSc patients does not change the circulating $CD4^+$ T-cell epigenome.

Sex differences contribute the greatest variance in the circulating $CD4^+$ T-cell regulome in SSc patients

The prevalence of autoimmune diseases, in particular SSc, is higher in females than males (Peoples et al., 2016). This observation is corroborated with the PCA results of our study participants that show that the greatest variance arises from biological sex differences (**Figure 1B, Figure 3A**) with 82 of 203 (40.4%) differential peaks arising from the X chromosome in females with SSc, 4 and 80 (1.2% and 24.8%) of 323 mapping to the X and Y chromosomes, respectively, in males with SSc, and the remaining differential peaks to the autosomes (**Supplementary Figure 3A**). To focus the differential analyses on sex differences exclusively, we compared only SSc females and males at baseline (if treated, or first available timepoint if treatment naïve) and were able to find clear segregation of gene regions more accessible in females with SSc that were distinct from those in males with SSc (**Figure 3B, 3D**).

General population (healthy control) data were obtained through published $CD4^+$ T-cell ATAC data (Qu et al., 2015) and analyzed separately from our SSc data to provide a comparison basis for sex-related differences unrelated to disease. Interestingly, there were fewer differential peaks arising from sex differences in the general population (Females = 54, Males = 154) and a larger fraction of differential peaks arose from the sex chromosomes (Female X = 77.8%, Male Y = 39.0%) than in SSc males and females (**Supplemental Figure 3B**). This disparity suggests that factors other than the sex chromosomes may drive the sex differences observed in SSc.

GREAT analysis of the differential peaks identified high prevalence of multiple immune-related pathways. In particular, T-lymphocyte-related programs associated to peaks more accessible in SSc males than SSc females (**Figure 3C**). Similarly, overlapping differential ATAC-seq peak regions to HiChIP anchor sites identified significant motif enrichment of genes involved in immune response and increased T-cell activation (AP-1, FOS, JUN, BATF) that are present in SSc males but not in any of the other groups (**Figure 3E**) and the Th2-activator GATA3 is significant in males in the volcano plot comparison of differentially accessible gene regions (**Figure 3F**). Moreover, enrichment of Th2-related activity in SSc males is supported by CIBERSORT analysis of the $CD4^+$ T-cell subtypes which revealed a trend (p-value=0.23) of a higher proportion of pathogenic Th2 cells compared to SSc females (**Supplemental Figure 3E**). Conversely, SSc females do have a significantly higher proportion of the more undifferentiated naïve T effector cells (**Figure 3G, 3H**). These differences are not present between the sexes in the general population

(**Figure 3I, Supplemental Figure 3F**), suggesting that divergences in differentiation and homeostasis of T effector cells may play a role in the sex differences observed in SSc.

In contrast, in separate analyses of healthy and SSc females, many of the same predicted cis-regulatory functions appeared in both groups and neither group showed motif enrichment of the SSc male-associated chromatin regions (**Figure 3C, Supplementary Figure 3C**, **Figure 3E**). Since biological females develop autoimmune diseases more commonly than males, this result is not surprising. Furthermore, males who develop SSc tend to have much more severe disease than females (Allison and Eugui, 2000; Peoples et al., 2016), supporting the hypothesis that more changes in immune-related expression are required to push males from homeostasis to disease.

Aging does not significantly alter chromatin accessibility in SSc peripheral T-cells

It is well-documented that aging changes the immune system and immune responses (Castelo-Branco and Soveral, 2014; Haynes, 2020; Müller et al., 2019). SSc is primarily a disease of adulthood, and our study did not have subjects <30 years old (**Table 1**). In our SSc study, age is a potential differential contributing factor that arises when sex-related differences are excluded from the comparison (**Figure 1B, Supplemental Figure 1E**). In contrast with sex, age-related differential peaks were more evenly distributed across both autosomes and sex chromosomes (**Supplemental Figure 3G**). Also, for age-specific analyses we included only treatment-naïve or at baseline patient samples to avoid potentially confounding factors (**Supplemental Figure 4**).

We observed a trend of increased chromatin accessibility in circulating $CD4^+$ T-cells with advancing age (**Supplemental Figure 4A**). Heat maps of accessible peaks revealed two distinct clusters corresponding to genes more accessible in younger versus older patients (**Supplemental Figure 4B**). The accessible genes comprising the older patients' cluster were related to immune activity pathways, such as the JUN-AP1 and BACH2-BATF motifs, interferon response factor IRF2 and T-cell proliferation regulator TNFSF8 (**Supplemental Figure 4C, D**). CIBSERSORT assignment of the $CD4^+$ T-cell subsets based on ATAC-seq signatures did not display any statistically significant or consistent trends between the three age categories (**Supplemental Figure 4F**). These findings are in line with previous findings of immune system aging (Keenan and Allan, 2019) and indicate that the effects of aging on $CD4^+$ T-cell chromatin accessibility is not a major mechanism of SSc pathobiology.

Serum autoantibody profiles are correlated with Th2-related pathways in SSc

Serum autoantibodies in SSc patients were the most significant non-sex related factor associated with $CD4^+$ T-cell ATAC-seq peaks (**Figure 1B, Supplemental Figure 1E**). When patients were grouped by autoantibody profile, the most pronounced peak differences were observed at the latest time point collected (data from 3rd timepoint shown), potentially because of prolonged disease progression. Thus, we utilized the third timepoint data for subsequent autoantibody-related analyses. Additionally, we included all patients with available ACA and RNAIII antibody data since there was very little overlap of total differential peaks across timepoints between each of the comparison factors (i.e., age, sex, treatment, etc., **Figure 1C**, **Table 1**).

ACA and RNAIII antibodies are mutually exclusive in > 95% of patients (Domsic and Medsger, 2016) and are associated with different clinical outcomes (e.g., pulmonary arterial hypertension and scleroderma renal crisis most commonly present in ACA and RNAIII-positive

SSc patients, respectively) (Nguyen et al., 2010; Odler et al., 2018; Steen et al., 2007). Given these clinical attributes, the lack of a significant number of Scl70 patients, and the consistent presence of ANA in nearly every patient, we focused our autoantibody analyses on differences arising from ACA and RNAIII expression (**Table 1**). A point of interest comes from patient 1837, who was not included in our ACA analysis due to lack of an ACA confirmatory test. However, since patient 1837 has confirmed expression of RNAIII autoantibodies, we can reasonably infer the absence of ACA (Domsic and Medsger, 2016). Furthermore, the ATAC-seq profile of subject 1837 clustered independently with the ACA negative patients, suggesting that chromatin accessibility profiles may predict autoantibody expression.

There was a clear distribution pattern of accessible DNA elements in $CD4^+$ T-cells in positive- compared to negative-ACA patients (**Figure 4A, C**). GREAT analysis of cis-regulatory functions of differential peaks revealed that more accessible peaks corresponded to Th2, cell-mediated immune responses, and T-cell differentiation in ACA+ patients (**Figure 4B**). Overlap of differential peaks with Hi-ChIP anchor sites in $CD4^+$ T-cell subsets showed enrichment of multiple motifs corresponding to immune cell function and autoimmunity (ETS family) (Garrett-Sinha et al., 2016), T-cell development (FLI1), Th2 differentiation (GATA3) as well as other immune cell programs (PU.1) that are significantly present in ACA+ T-cells but not ACA- T-cells (**Figure 4D**). Regions of genomic accessibility corresponding to the pro-inflammatory transcription regulator, NFKB1, and Th2 genes, IL4, IL4R, and IL21R, associated with ACA+ (**Figure 4E**). Additionally, CIBERSORT analysis showed that $CD4^+$ T-cell subset composition was significantly different between ACA+ and ACA- patients (**Figure 4F**), with a much higher percentage of Th2 cells in ACA+ compared to ACA- patients (**Figure 4G**).

Next, we sought to determine the relationship between peaks in patients with different serum autoantibodies. As in the ACA comparison group, there was a clear distribution pattern distinguishing RNAIII+ and RNAIII- genomic accessibility in $CD4^+$ T-cells (**Figure 5A, C**). Upon closer examination of genomic regions and associated pathways, there were clear similarities shared between ACA- and RNAIII+ patients even though not all ACA- patients are also RNAIII+, as some patients were negative for both autoantibodies (ACA-/RNAIII-). Similar to the ACA+ group, a subset of RNAIII- patient cells showed greater and more differential peaks at the genomic accessibility level as analyzed by ATAC-seq compared to RNAIII+ associated peaks (**Figure 5A**). These two different peak sets (RNAIII+ and RNAIII-) gave rise to two distinct clusters on the Z-score heatmap (**Figure 5C**).

Furthermore, GREAT analysis revealed that CD4+ T-cells from ACA+ and RNAIII- patients shared many immunity and T-cell related pathways, particularly Th2 differentiation (**Figure 5B**) and the volcano plot of significant RNAIII- differential peak regions highlighted Th2-related genes such as IL4, IL4R, and IL21R (**Figure 5D**). These attributes were corroborated with CIBERSORT breakdown of the $CD4^+$ T-cell subset that once again highlighted the significant difference in Th2 composition in RNAIII+ and RNAIII- cohorts. Both ACA+ and RNAIII- groups contained higher Th2 percentages when compared to their respective counterparts (**Figure E, F**). Additionally, the majority of differential peaks came from the ACA+ and RNAIII- groups while ACA- and RNAIII+ contributed fewer differential peaks (**Supplemental Figure 5A, B**), suggesting that major autoantibody-related differences primarily arise from ACA+ and/or RNAIII- carriage status.

Anticentromere antibodies may be predictive of Th2-mediated fibrosis in SSc

We have shown that CD4$^+$ T-lymphocytes in SSc patients that are ACA+ and/or RNAIII- evinced significantly higher proportions of Th2 cells and related motifs and regulatory pathways. There were 44 total genes in the overlap of differential peaks associated with both ACA+ and RNAIII-, of which 19 were shared with SSc males, and featured multiple Th2-related genes, such as *IL4* and *IL21R* (ACA+ and RNAIII- only) and *GATA3* and *IL4R* (shared with SSc males) (**Figure 6A**). Here, we focus on the *IL-4-KIF3A* and *IL4R-IL21R* regions, which were previously identified as associating with ACA+ and RNAIII- in the volcano plots (**Figure 4E, Figure 5D**).

Th2 cells produce both IL-4 and IL-13 to stimulate fibrosis. The *IL-4* gene locus is in close genomic proximity to both *IL-13* and *KIF3A* (**Figure 6B**), another gene shared by the Th2-high groups (ACA+, RNAIII-). KIF3A is a ciliary protein important in myofibroblast development in SSc (Rozycki et al., 2014; Teves et al., 2019). The expected trends for accessibility in the *IL-4-KIF3A* genomic interval was reflected across all three comparison groups (females vs. males, ACA+ vs. ACA- and RNAIII+ vs. RNAIII-) in relation to predicted Th2 cell proportions: peaks were larger in males compared to females, and significantly larger in ACA+ compared to RNAIII+. We also identified an active enhancer located between *IL-13* and *KIF3A* that is predicted through HiChIP to interact with *IL-4, IL-13*, and *KIF3A* in Th17 and Treg cells (**Figure 6B**). The peak levels of this putative enhancer also reflect predicted Th2 activity levels.

Examination of *IL4R* locus in the *IL4R-IL21R* genomic region showed a similar accessibility pattern as the *IL4* region with higher accessibility peaks in samples with higher proportions of Th2 (**Figure 6C**). *IL21R* neighbors *IL4R* and also displays more chromatin access in the Th2-high ACA+ CD4$^+$ T-cells compared to the Th2-low RNAIII+ CD4$^+$ T-cells (**Figure 6C**). IL21R is the receptor for IL-21, a potent cytokine secreted by both pathogenic Th2 and Th17 cells that promotes Th17 differentiation, inhibits Th1 differentiation, and drives fibrosis in diseases of chronic skin inflammation as well as pulmonary fibrosis in SSc (Brodeur et al., 2015; Costanzo et al., 2010; Kastirr et al., 2014; Lei et al., 2015; Sarra et al., 2011; Wurster et al., 2002). Interestingly, patients without either ACA or RNAIII antibodies (double negative) possessed accessibility levels falling at an intermediate level between the higher ACA+ and lower RNAIII+ peak levels in both the *IL13-KIF3A* and *IL4R-IL21R* regions (**Figure 6B, C**), suggesting that expression of either autoantibody influences Th2-cytokine genomic accessibility, and potentially expression, patterns.

Our results suggest an association between ACA+ and/or RNAIII- autoantibody status and higher Th2 prevalence and Th2-cytokine activity in SSc patients and suggest autoantibody profiles impact circulating cellular pathway activation in patients with SSc. Furthermore, previous studies have identified Th2 cells as a driving force behind fibrosis in SSc (Chizzolini et al., 2003; Mavalia et al., 1997). Taken together, the higher Th2 cell proportions and activity signatures detected in ACA+ and RNAIII- patients in this study may explain differences in observed clinical phenotypes.

DISCUSSION

Herein, we have comprehensively analyzed the chromatin landscape of circulating CD4+ T-lymphocytes in a longitudinal study of 18 SSc patients across multiple clinical variables. While patient age did not significantly correlate with differences in CD4 T-cell chromatin accessibility, we did find the well-established SSc biological sex bias to underly significant differences in the SSc chromatin landscape. We included the whole genome in our study, expanding from existing studies on SSc sex biases focusing exclusively on X-linked SNPs and X-linked epigenetic modifications (Saveria Fioretto et al., 2020). Importantly, we have identified a novel correlation

of serum ACA positivity to fibrosis-driving Th2 cells, including a prospective pathway of cytokine involvement connected with PAH development.

ACA and RNAIII are autoantibodies highly specific for SSc rarely expressed in healthy individuals with low prevalence in other diseases (Clark et al., 2022). Serum autoantibodies are currently used as predictive tools for disease outcome as ACA patients tend to have lower early mortality but greater likelihood for developing PAH while RNAIII patients are more likely to experience earlier lethality and renal crisis (Domsic and Medsger, 2016). However, mechanisms to explain the association between the presence of serum autoantibodies in SSc patients with specific outcomes remains murky. We have therefore advanced a critical missing link in connecting ACA positivity to increased Th2 fractions and fibrotic cytokine activity.

The Th2 cytokines IL-4 and IL-13 are both detected at higher serum levels in SSc patients (Allanore et al., 2020b; Gasparini et al., 2020), and have been implicated as drivers of PAH (Christmann et al., 2011; Kumar et al., 2015; Soon et al., 2010; Sweatt et al., 2019). Combined with the clinically-documented association between ACA+ and PAH development (Domsic and Medsger, 2016), these results support our proposed model that ACA carriage is connected to the Th2 fibrosis-promoting pathway whereas RNAIII carriage is associated with an alternative pathway involving less Th2 activity (**Figure 6D**). Additionally, in the tight skin scleroderma mouse model, IL-4 has been strongly linked to dermal fibrosis: IL-4 $^{-/-}$ mice display less skin fibrosis (Ong et al., 1999) and addition of anti-IL-4 antibody reduces collagen production in IL-4 stimulated tight skin dermal cells (Ong et al., 1998). CD8+ production of IL-13 is directly correlated with dermal fibrosis in SSc patients (Fuschiotti et al., 2013; Fuschiotti et al., 2009). Together with our data correlating ACA+ but not RNAIII+ to increased chromatin accessibility to the *IL13-IL4* genomic loci, autoantibody profiles may, thus, not only be used as a predictive diagnostic tool for internal organ involvement such as PAH or renal crisis, but also fibrotic severity in SSc patients when combined with tracking of Th2-cytokines and cellular fractions.

MMF is an immunosuppressive drug that is used in autoimmune diseases for its immunomodulatory effects. However, we showed here that MMF treatment does not confer any significant changes to the chromatin state of circulating T-cells over the time course of our study (**Figure 2**). It is possible that MMF works on the tissue level and/or other cell type(s) (e.g., macrophages (Hinchcliff et al., 2018)) rather than the CD4 T-cell epigenome or requires a longer time period to show an effect. Our study results suggest that targeted therapies to modulate Th2 activity can potentially be a specific and effective treatment option for ACA+ and/or for male patients with high levels of Th2-cytokines. In particular, IL-4 and IL-13 have emerged as promising therapeutic targets in SSc (Gasparini et al., 2020), and two drugs are in clinical trials: (1) Dupilumab (DB12159), an anti-IL-4 and IL-13 monoclonal antibody used to treat atopic dermatitis, is currently in Phase II trials for localized SSc (trial identifier: NCT04200755, 2019-002036-90, Uni-Koeln-3815) and (2) romilkimab (SAR156597), an IL-4 and IL-13 neutralizing IgG bi-specific antibody that appears to significantly improve skin fibrosis based upon the results of an early Phase II trial in patients with early dcSSc (Allanore et al., 2020b). And given the recent trend towards adding immunomodulatory therapies, such as rituximab, to PAH-specific therapies in SSc-PAH (Clinicaltrials.gov identifier: NCT01086540) (Prins et al., 2019; Zamanian et al., 2021), it will be useful to explore if targeting IL-4/IL-13 in SSc-PAH patients, particularly those who are ACA+, is a more direct approach than adjunctive therapy. Moving forward, future trials of targeted therapies should include SSc autoantibody expression for consideration.

Herein, we have demonstrated that ATAC-seq is a powerful and sensitive tool capable of high-fidelity detection of distinct open chromatin signatures that are associated with individual SSc-specific serum autoantibodies. ATAC-seq analysis of $CD4^+$ lymphocytes was sufficient to consistently group each patient both by sex and by autoantibody profile. From our pathway analysis, we predict that future clinical studies involving ACA+ SSc patients and anti-IL-4 and anti-IL13 therapy will be promising avenues to explore. Future experiments will further expand investigation into other SSc autoantibodies, such as pathways related to RNAIII+ and Scl70+, and the involvement of other immune cell types, such as B-cells and myeloid cells.

The expansion of ATAC-seq datasets into larger sample sizes, more cell types, additional SSc autoantibodies and clinical disease traits (i.e. mRSS, limited or diffuse subset, organ involvement, and etc.) will power the development of robust machine learning models that may be used to analyze a single sequencing sample at high confidence. These dataset models will not only provide pathway and predictive disease information, but also replace multiple invasive and expensive clinical visits and tests. In a chronic and painful disease such as SSc, where epidermal and vascular stiffness can complicate even standard venipunctures, reducing the amount of blood and biopsies needed for evaluation and diagnosis will immediately improve standard of care. Furthermore, while this particular study focused on SSc patients, the technological applications and analysis used and advancements discovered here can be applied to the investigation of other autoimmune diseases.

ACKNOWLEDGEMENTS

We thank members of the Chang lab and Dr. Oliver Distler for discussion. This work was supported by Scleroderma Research Foundation (H.Y.C.), NIAMS T32 AR007422 (D.R.D.), NIAMS T32 AR050942 (B.T.A.), NICHD K12 HD055884 (M.H.), NIAMS K23 AR059763 (M.H.), NIAMS R01 AR073270 (M.H.). H.Y.C. is an Investigator of the Howard Hughes Medical Institute.

AUTHOR CONTRIBUTIONS

Conceptualization: D.R. Dou and H.Y. Chang; Methodology and Investigation: D.R. Dou, Y. Zhao, K. Aren, M. Carns, and R. Li; Data Analysis: D.R. Dou, Y. Zhao, and B. Abe; Writing: D.R. Dou, Y. Zhao, B. Abe, L.C. Zaba, L.S. Chung, M. Hinchcliff, and H.Y. Chang; Funding Acquisition: H.Y. Chang M. Hinchcliff; Resources: M. Hinchcliff and H.Y. Chang; Supervision: M. Hinchcliff, and H.Y. Chang.

COMPETING INTERESTS

H.Y.C. is a co-founder of Accent Therapeutics, Boundless Bio, Cartography Biosciences, Orbital Therapeutics, and an advisor to 10x Genomics, Arsenal Biosciences, Chroma Medicine, and Spring Discovery. M.H. has received consulting fees from AbbVie and Boehringer Ingelheim.

MATERIALS & CORRESPONDENCE

Further information and requests for resources and reagents should be directed to and will be fulfilled by the lead contact, Howard Y. Chang (howchang@stanford.edu). Queries about the clinical cohort in this study should be directed to the co-lead contact, Monique Hinchcliff (monique.hinchcliff@yale.edu).

METHODS:

Clinical Cohort

The Northwestern University Institutional Review Board approved the study (IRB# STU00080199), and SSc patient participants provided informed consent in accordance with the Declaration of Helsinki. Patient participants fulfilled 2013 American College of Rheumatology SSc (van den Hoogen et al., 2013), or three out of five CREST (calcinosis, Raynaud, esophageal dysmotility, sclerodactyly, telangiectasias), criteria. Research participants' blood samples were collected in green-topped tubes containing sodium heparin. A subset of SSc patients were commencing mycophenolate mofetil (MMF) for a clinical indication at 250 mg PO BID with dose escalation to 1000-1500mg PO BID as tolerated. One physician performed clinical exams including mRSS (LeRoy et al., 1988). Serum autoantibodies were measured by indirect immunofluorescence at Specialty Laboratories, Valencia, CA. Subsequent blood collection for research was performed at the time of clinically indicated testing.

$CD4^+$ T-cell isolation and ATAC-seq library preparation

Lymphocyte isolation for ATAC-seq library preparation was performed as previously described (Qu et al., 2015). 5mL of whole blood was enriched for $CD4^+$ cells using RosetteSep Human CD4+ T Cell Enrichment Cocktail (StemCell Technology). $CD4^+$ cells were frozen in 10% DMSO/FBS and stored in liquid nitrogen. Frozen cells were thawed and washed twice in 5% FBS in PBS1x, filtered through 100 uM cell strainers, stained for viability with 7-AAD (BD Biosciences, 559925), and T-cell markers mouse anti-human CD3 (Thermo Fisher Scientific, 11-0037-41) and mouse anti-human CD4 (Tonbo Biosciences, 20-0048-T025), and sorted for live 7-AAD^- $CD3^+$ $CD4^+$ T-lymphocytes using the BDFACS ARIA II with a 100 uM nozzle. After $CD4^+$ cells were sorted, 50,000 $CD4^+$ T cells were used for Omni-ATAC library prep (Corces et al., 2017). Sequencing library quality metrics are included in **Supplemental Table 2** and visualized in **Supplemental Fig. 1**.

Mitochondrial mutation calling and patient samples consistency confirmation

We used the mitochondrial mutation information to confirm consistent identity of patients across timepoints using the previously described mitochondrial SNP pipeline (Xu et al., 2019). The GRCh37 reference from the 1000 Genomes Project and the mtDNA sequence rCRS (revised Cambridge reference sequence) were used for mitochondrial mutation calling pipeline. Paired-end ATAC-seq fastq files were first aligned to the reference genome using BWA (Li and Durbin, 2009). Reads aligned to the mitochondria reference genome were then extracted. Samtools (Li et al., 2009) was used to convert mitochondrial sam files to bam files, sort bam files, and remove duplicated reads. Samtools mpileup was used to generate the pileup file for each sample with option "-q 30 -Q 30". A custom perl script was used to get mutation information from pileup file and filter low quality reads. SNPs with allele frequency larger than 0.9 and support reads larger than 3 were selected. A heatmap was used to check whether the mitochondrial mutation is consistent across samples from three timepoints for each patient **(Supplemental Fig. 1A**).

ATAC-Seq data Analysis

The adaptor of paired-end ATAC-seq data were first trimmed by an in-house software, and then aligned to hg38 genome using bowtie2 (Langmead and Salzberg, 2012). The mitochondrial reads

and reads with low alignment score (<10) were removed. The aligned sam files were converted to bam files and sorted by Samtools. Picard (http://broadinstitute.github.io/picard/) was used to remove duplicate reads and Macs2 was used to call peaks (Zhang et al., 2008). Each ATAC-seq peak was annotated by its nearby genes using GREAT (McLean et al., 2010) under the basal plus extension default setting. Bam files were converted to bedGraph format using the Bedtools genomeCoverageBed module (Quinlan and Hall, 2010). After normalization by total reads, bedGraph files were converted to BigWig format using the bedGraphToBigWig module from ucscTools (Kent et al., 2010) for visualization purpose. The bedtools MultiBamCov module was used to generate read count matrix from bam files.

Differential ATAC-seq peaks were identified using the negative binomial models from the R package DESeq2 (Love et al., 2014). The Benjamini hochberg procedure (Benjamini and Hochberg, 1995) was used to adjust for multiple hypothesis testing. Peaks with FDR < 0.2 and absolute fold change larger than 1.5 were selected as significant for Sex and Age factors. Peaks with FDR < 0.3 and absolute fold change larger than 1.5 were selected as significant for ACA and RNAIII comparisons.

Healthy control CD4 T cell ATAC-seq data were downloaded from GEO (GSE85853) (Qu et al., 2017). When comparing males with females, we used the same methods to analyze the healthy control samples as we did in the SSc sample data set. However, due to concern for batch effects, downloaded healthy control data were compared only with each other and not directly with the SSc group samples from our study.

CIBERSORT analysis

CIBERSORT (Newman et al., 2015) was used to estimate the abundance of CD4 T cell subtypes in bulk ATAC-seq data. First, the reference CD4 T cell ATAC-seq peaks and according read count matrix were downloaded from GEO (GSE118189 (Calderon et al., 2019)). The Bedtools intersect module was then used to identify the overlap peak set between the SSc ATAC-seq peaks and reference peaks. The overlap peak set, mixture file, reference sample file, and phenotype files were generated according to the CIBERSORT manual. The R package edgeR (Robinson et al., 2010) was used to normalize both Mixture count matrix and reference count matrix, and the subsequent matrices converted to log2CPM value. The signature file and the final CD4 T cell subtypes fraction matrix were then generated using CIBERSORT.

GWAS enrichment analysis and GO term analysis

We gathered known GWAS SNPs from the European Bioinformatics Institute GWAS catalog (https://www.ebi.ac.uk/gwas/docs/file-downloads), and retrieved index SNPs associated with autoimmune and control diseases. We then retrieve linked SNPs with Linkage Disequilibrium (LD) $r^2 > 0.8$ to the index SNPs. This LD information was obtained from the haploreg website (http://archive.broadinstitute.org/mammals/haploreg/data/). The uscsTools liftOver module was used to lift SNP positions over to the hg38 genome. The numbers of SNPs within the SSc ATAC-seq peak regions were calculated for each disease. Random peaks were sampled from genome using the bedtools shuffle module with the same size of SSc ATAC-seq peaks and the number of SNPs within the random peak regions were subsequently recorded. The random

shuffle procedure was conducted 1000 times to construct a null background, and the empirical p values were then respectively computed. The fold enrichment of GWAS analysis was calculated as the observed number of overlapping SNPs versus the mean random shuffled background.
SSc GWAS SNPs within our SSc ATAC-seq data were recorded as SSc ATAC-specific GWAS SNPs. Identities of these specific associated SNPs were assigned in accordance to nearby genes and then were passed to Gprofiler (Raudvere et al., 2019) for functional gene set enrichment analysis.

HiChIP data Analysis

HiChIP data for all valid pair matrices for Naïve T cells, Th17 cells and Treg were downloaded from GEO (GSE101498 (Mumbach et al., 2017)). H3K27ac ChIP-seq peaks for Naïve T cells, Tregs and T helper cells were downloaded from ENCODE as 1d peak sets. The FitHiChIP (Bhattacharyya et al., 2019) pipeline was used to call loops with 5kb bin, peak-to-all interaction type, loose background, and FDR < 0.01. LiftOver was used to convert the merged significant interaction files generated from the FitHiChIP pipeline from hg19 to hg38, the hg38-aligned files were then converted to BigBed format as described in the FitHiChIP online manual (https://ay-lab.github.io/FitHiChIP/usage/output.html) and visualized in UCSC web browser.

Motif analysis

Homer (Heinz et al., 2010) was used to conduct motif enrichment analysis using the intersecting regions between SSc ATAC-seq peaks and significant 5kb binned loops anchors called by FitHiChIP pipeline. Motifs with FDR < 0.05 were considered significant for each comparison.

Statistical Analyses

All statistical analyses and quantification were conducted in R or GraphPad Prism. Differential peaks were calculated using negative binomial models. Where applicable, p-values are indicated on the figures; multiple hypothesis testing is controlled for using the Benjamini-Hochberg method to estimate false discovery rate (FDR). Non-significant comparisons, including those rejected based on FDR, are indicated with “NS” on the figure. Figure legends state the statistical details of the experiments and assays, including exact “n” values, statistical tests, comparisons, and cutoffs specifically used in each figure.

Data Availability

All ATAC-seq files and processed files for this study have been deposited in the Gene Expression Omnibus (GEO) under the accession identifier GSE163066.

MAIN FIGURES

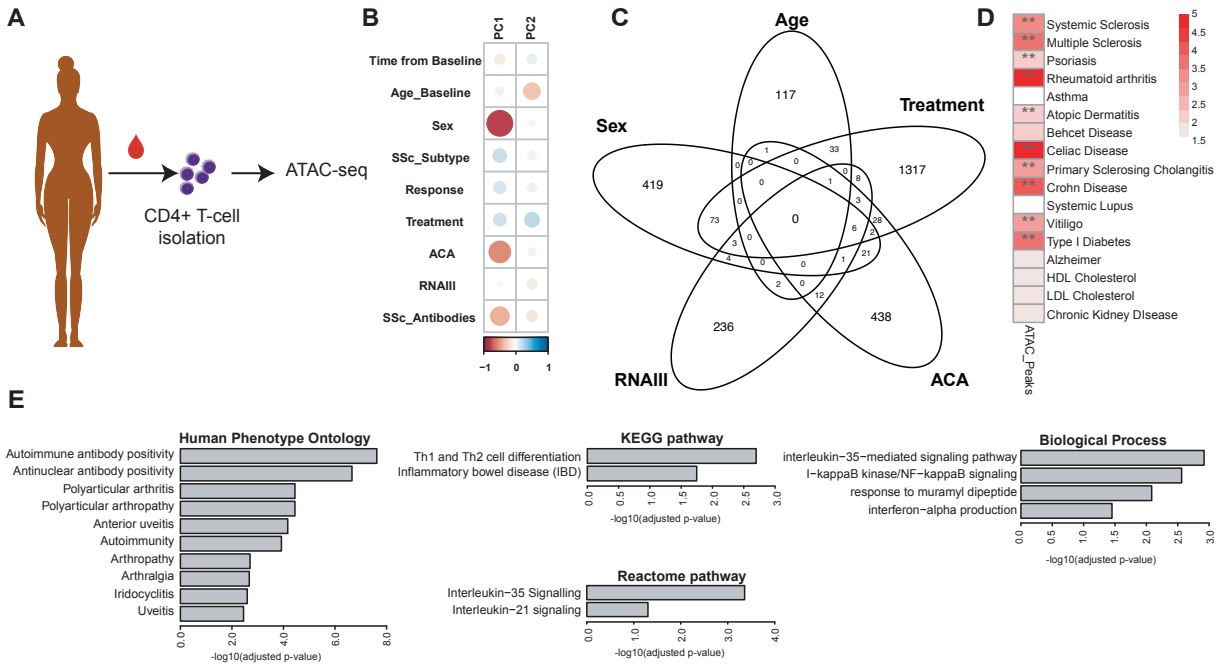

Figure 1: *General characteristics of SSc study patients*. **A** Diagram of sample collection from patients and ATAC-seq library preparation of CD4$^+$ cells. **B** Spearman Correlation between PC1/PC2 and each contributing variable tested, color indicates spearman correlation value (from -1 red to 1 blue), size indicates strength of correlation (larger is stronger). **C** Differential peaks across all timepoints and samples for each of the main variables. **D** enrichment of GWAS SNPs in open chromatin regions from the SSc study samples to verified autoimmune disease-associated SNPs. Scale bar corresponds to fold enrichment of SNPs in diseases compared to the random sampling background (red=high enrichment, white = low enrichment), ** indicates FDR < 0.05 and fold enrichment > 2. **E** GO term and pathway analysis of SSc SNPs enriched ATAC peaks associated genes. ATAC-seq data analyzed using DESeq 2, statistics calculated using negative binomial modeling. N=18 patients across 3 timepoints each (see **Supplementary Tables 1** and **2**)

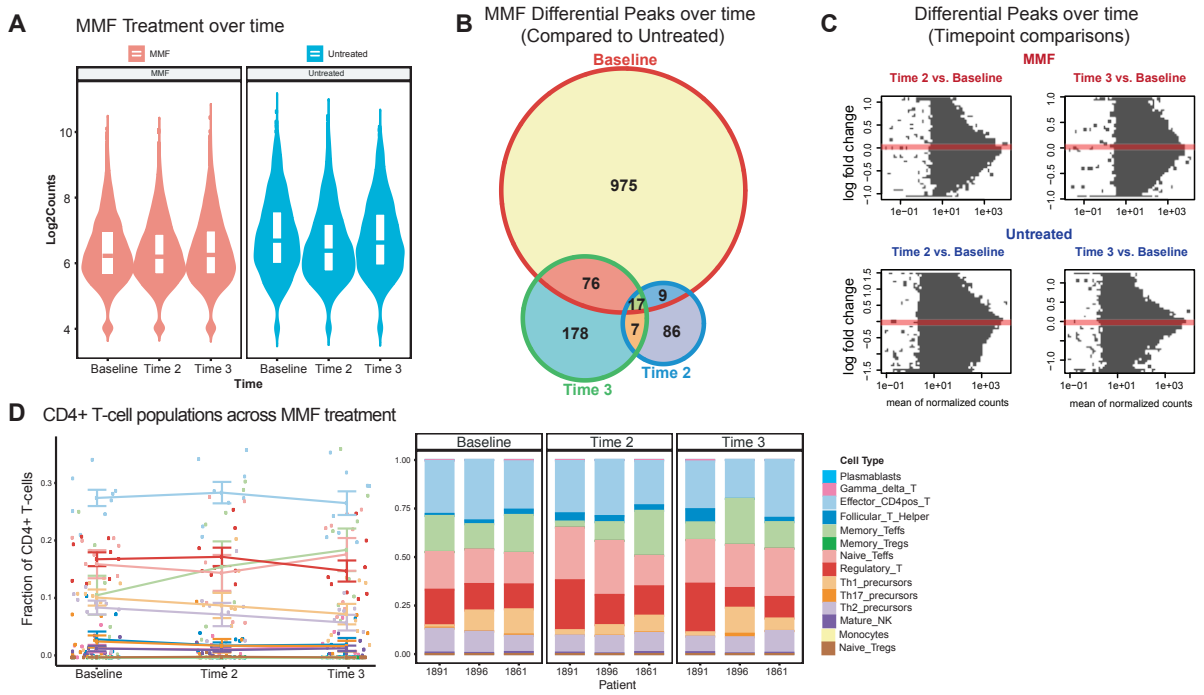

Figure 2: *MMF treatment has no significant effect on CD4+ epigenome in SSc study patients*. **A** Violin plot of differential ATAC peaks between MMF vs. healthy across all three timepoints in MMF-treated (red) and treatment naïve (blue) SSc patients. **B** Venn diagram of number of differential peaks in MMF-treated patients as compared to treatment naïve (untreated) across timepoints. **C** MA plots of differential peak comparisons between timepoints in both MMF-treatment and untreated groups. Red dots indicate significance. **D** CIBERSORT analysis of $CD4^+$ T-cell subsets in MMF-treatment patients across time (composite of all patients by cell type, left, individual patient examples, right). N=10 MMF-treated patients, N=4 Treatment naïve patients, all across 3 timepoints each

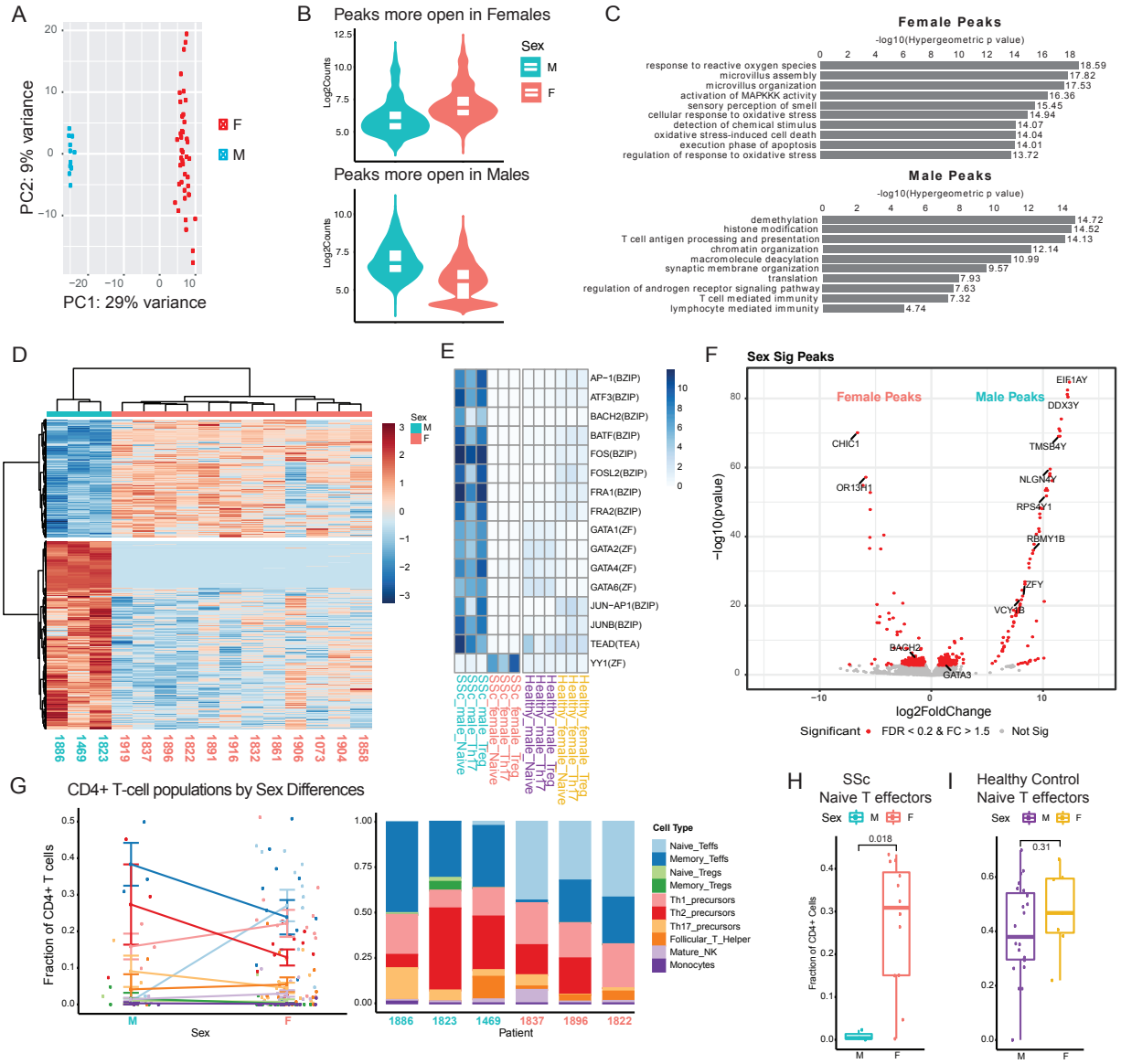

Figure 3: *Greatest variance in SSc study patients arises from sex differences*. **A** PCA analysis of all patients and all timepoints grouped by sex (N=18, across 3 timepoints each). **B** Violin plots depicting peaks more accessible in females (red) and in males (blue) (N=18, across 3 timepoints each). **C** GREAT predicted functions of cis-regulatory regions associated with peaks accessible in SSc females and males. P-values calculated using Fisher's Exact Test (N=18, across 3 timepoints each). **D** Heatmap of differential ATAC-seq peaks between male and female SSc study patients at treatment-naïve, baseline timepoint grouped by sex (red label = female, blue label = male), scale bar indicates z-score of accessibility (red is more accessible and blue is less accessible). P-values calculated using negative binomial models in DESeq2. **E** Heatmap of motif enrichment of the genomic region from overlay of significant ATAC-seq peaks with HiChIP anchors, scale bar indicate significance of enrichment (values correspond to -log10(p-value), darker blue is more significant) (SSc N=18, across 3 timepoints each; Healthy controls N=6). **F** Volcano plot of differential peaks with FDR < 0.2 and absolute fold change larger than 1.5 highlighted in red,

significance calculated using negative binomial models in DEseq2. **G** CIBERSORT analysis of $CD4^+$ T-cell subsets in male and female SSc patients (left panel: composite of N=17 patients across 3 timepoints each by cell type; right panel; individual patient examples). **H** Percentage of Naïve T effectors grouped by sex in SSc study patients (N=17, across 3 timepionts each) calculated by CIBERSORT **I** Percentage of Naïve T effectors in general population control patients calculated by CIBERSORT (N=6, 3 female and 3 male).

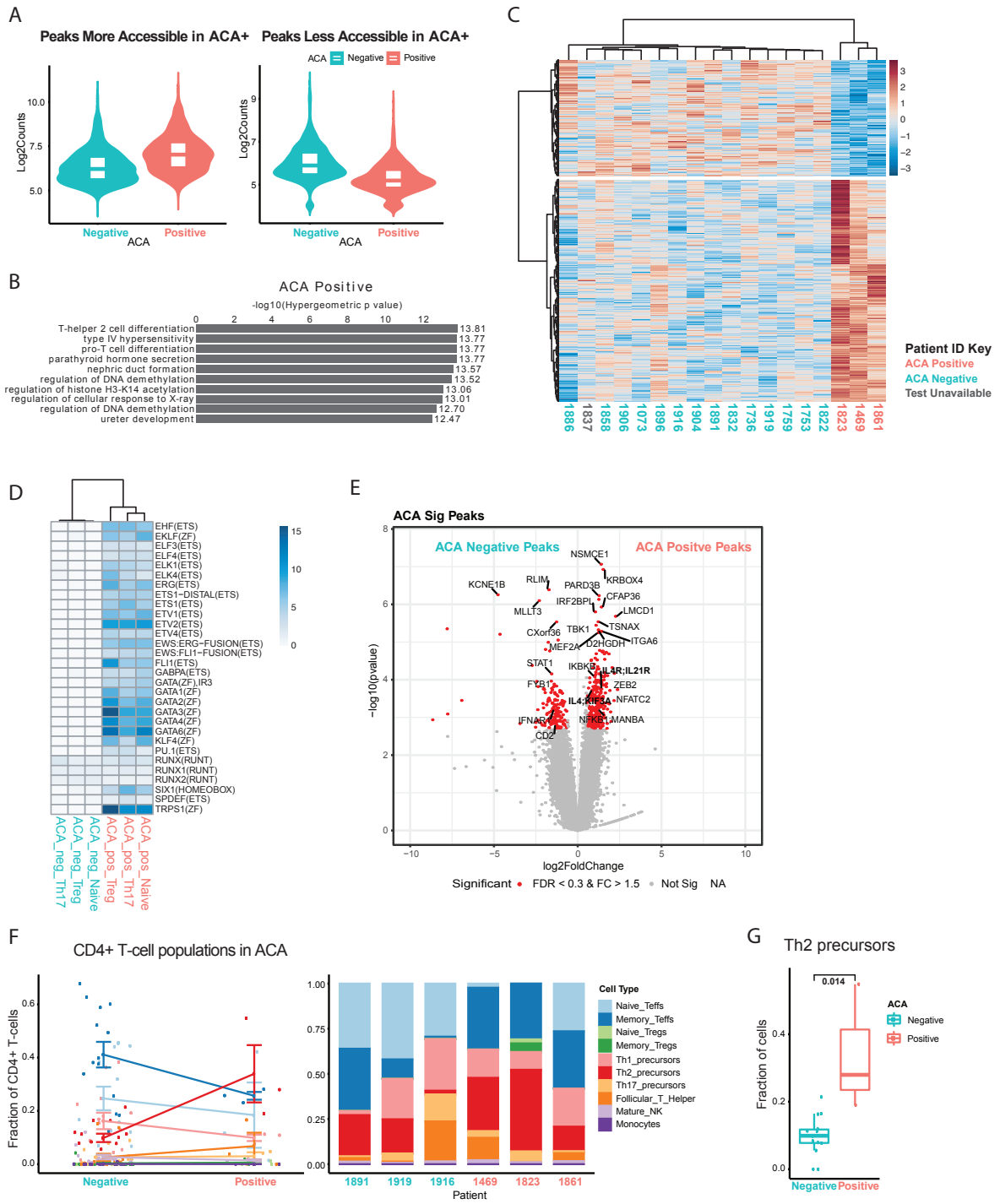

Figure 4: *ACA-positive patients present with more Th2 cells*. **A** Violin plots depicting peaks more accessible in ACA-positive (red) and in ACA-negative (blue) patients. **B** GREAT predicted functions of cis-regulatory regions associated with peaks accessible in ACA-positive patients (GREAT analysis for ACA-negative patients not significant). Statistics calculated using Fisher's Exact Test, N=18, 3 timepoints each). **C** Heatmap of differential ATAC-seq peaks of SSc study patients at latest timepoint (N=18, timepoint 3 shown) available grouped by ACA- positive (red) and negative (blue). Grey indicates status not reported. Scale bar indicates z-score of accessibility (red is more

accessible and blue is less accessible) **D** Heatmap of motif enrichment of the genomic region from overlay of differential ATAC-seq peaks with HiChIP anchors, scale bar indicate significance of enrichment (values correspond to -log10(p-value), darker blue is more enriched and significant. N=18 patients, 3 timepoints each. **E** Volcano plot of differential peaks with FDR < 0.3 and absolute fold change larger than 1.5 highlighted in red (N=18, 3 timepoints each). **F** CIBERSORT analysis of $CD4^+$ T-cell subsets in ACA- positive and negative patients (composite of all patients by cell type, left, individual patient examples, right). **G** Percentage of Th2 precursor cells grouped by ACA-status in SSc study patients (N=17, 3 timepoints each) calculated by CIBERSORT

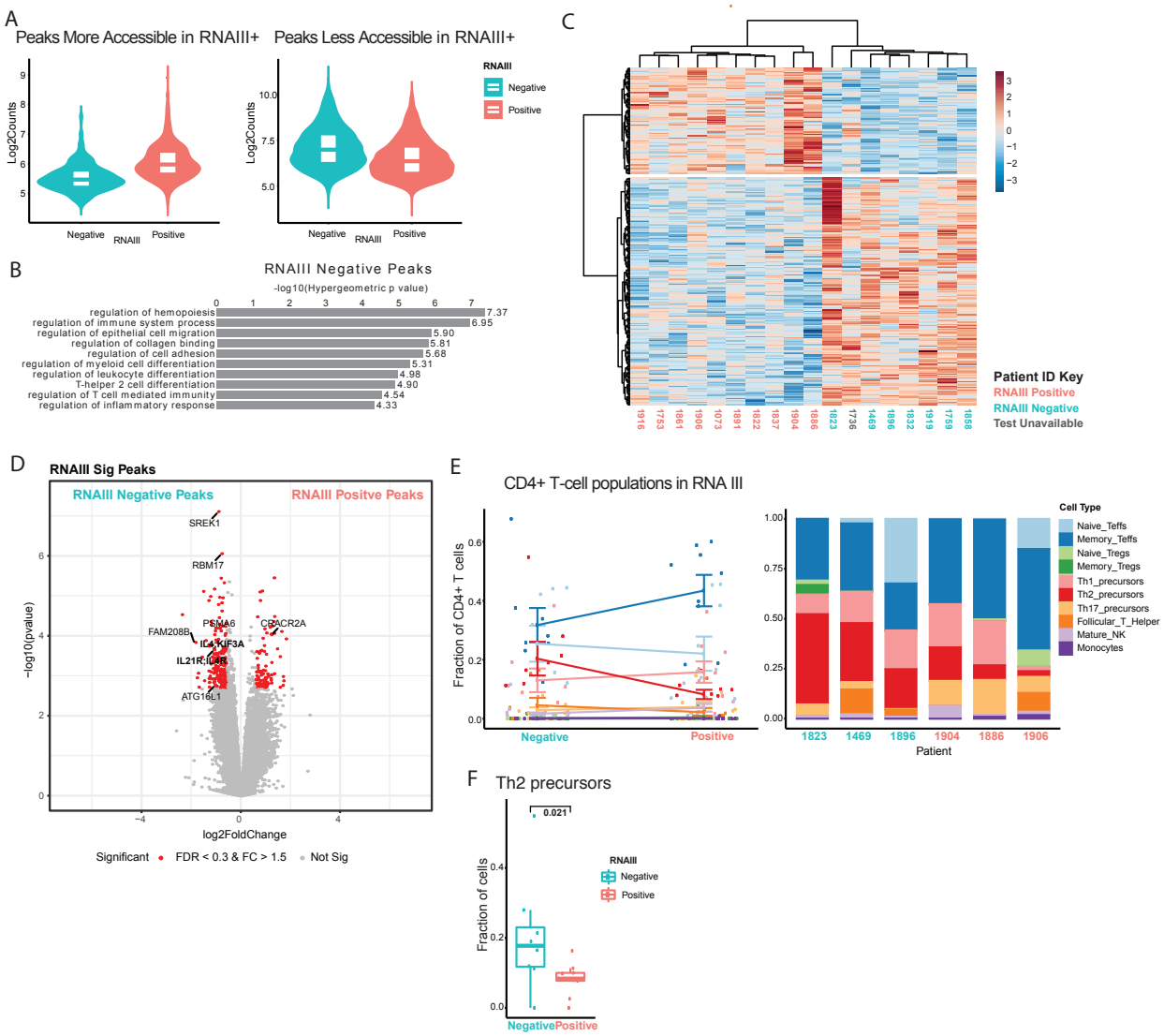

Figure 5: *RNAIII-positive patients present with fewer Th2 cells*. **A** Violin plots depicting peaks more accessible in RNAIII-positive (red) and in RNAIII-negative (blue) patients. **B** GREAT predicted functions of cis-regulatory regions associated with peaks accessible in RNAIII-negative patients (GREAT analysis for RNAIII-positive patients not significant). **C** Heatmap of differential ATAC-seq peaks of SSc study patients at latest timepoint (timepoint 3, N=18) available grouped by RNAIII-positive (red) and negative (blue). Grey indicates status not reported. Scale bar indicates z-score of accessibility (red is more accessible and blue is less accessible) **D** Volcano plot of differential peaks with FDR < 0.3 and absolute fold change larger than 1.5 highlighted in red. **E** CIBERSORT analysis of $CD4^+$ T-cell subsets in RNAIII- positive and negative patients (composite of all patients by cell type, left, individual patient examples, right). **F** Percentage of Th2 precursor cells grouped by RNAIII-status in SSc study patients calculated by CIBERSORT (Wilcoxon Rank Sum test, N=17, 3 timepoints each).

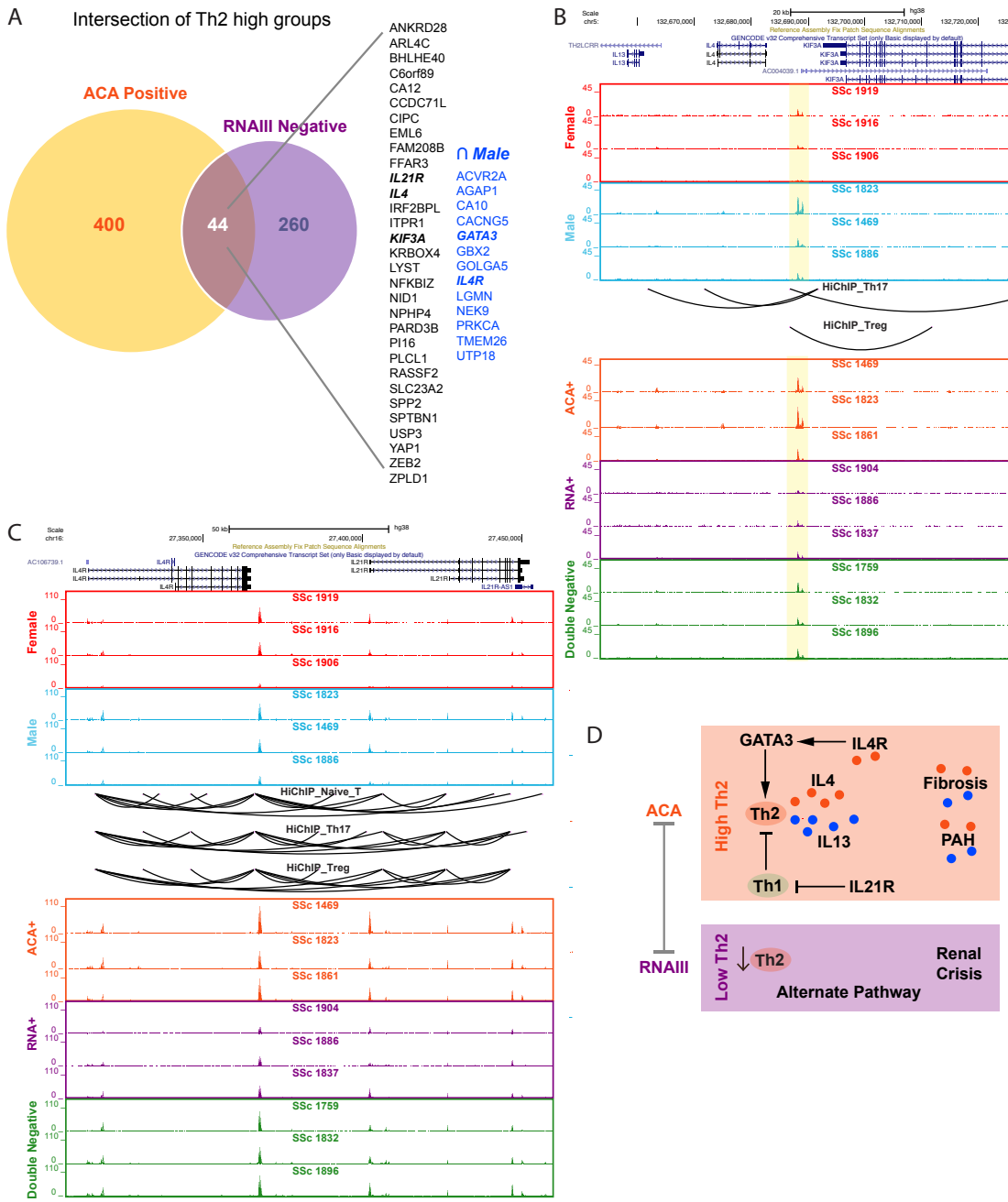

Figure 6: *Interplay between autoantibody groups and Th2 pathways*. **A** Venn diagram of accessible differential peaks in ACA-positive and RNA-negative SSc study patients (N=18 patients, 3 timepoints each). The genes within the intersection of the two autoantibody groups are listed and the intersection with male peaks are in blue. Bold italic indicates Th2-related genes. Representative ATAC-seq tracks for **B** the IL4;KIF3A and **C** the IL4R;IL21R genomic regions. Representative tracks for females at baseline (red), males at baseline (blue), ACA-positive at timepoint 3 (orange), RNA-III positive at timepoint 3 (purple), and ACA/RNAIII dual-negative at timepoint 3 (green) with HiChIP interaction loops from Naïve T-cell, Th17 and Tregs (black loops). The predicted enhancer for IL-13, IL-4, and KIF3A is highlighted in yellow. **D** Proposed model of relation between autoantibody expression and Th2 activation.

SUPPLEMENTAL FIGURES

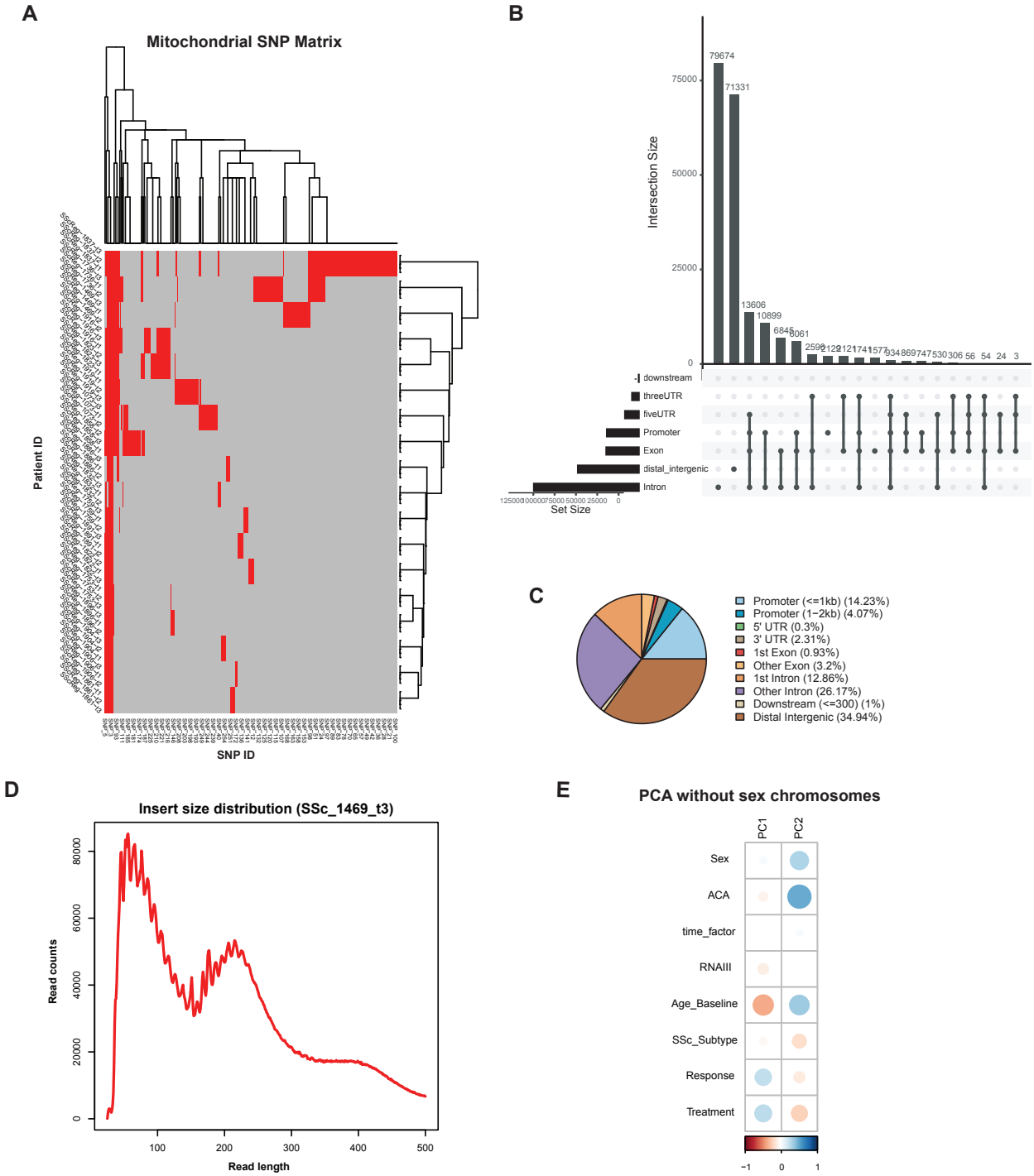

Supplemental Figure 1: *Quality check of ATAC-seq libraries for SSc study.* **A** Matrix of mitochondrial SNPs for every patient at every timepoint to confirm veracity of patient ID across the study. **B** Graph of ATAC-seq peak distribution by number of peaks. **C** Venn diagram of ATAC-seq peak distribution by percentages. **D** Representative plot of ATAC-seq library fragment length distribution (SSc_1469_t3). **E** PCA plots of contributing variables in the study, excluding peaks from the sex chromosomes (autosomes only). N=18, 3 timepoints each

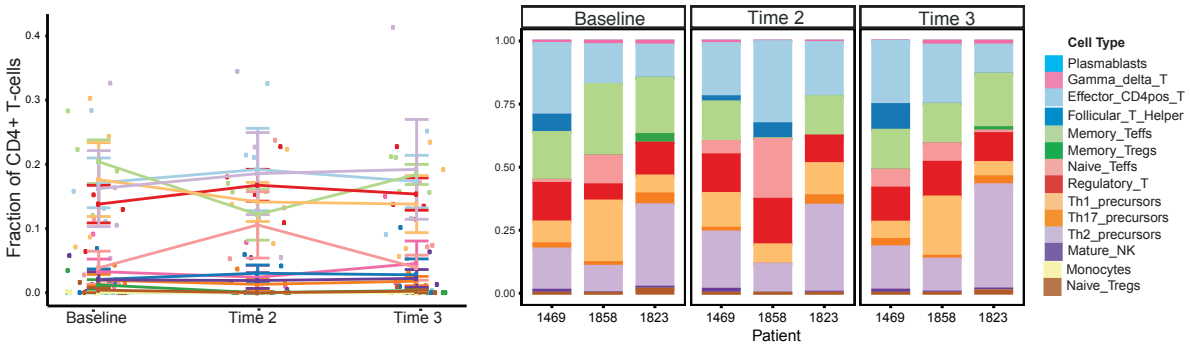

Supplemental Figure 2: CIBERSORT analysis of $CD4^+$ T-cell subsets in treatment naive SSc patients (Left panel: composite of all patients (N=17, 3 timepoints each) by cell type; Right panel: representative plots for 3 individual patient examples. Statistics calculated using the Wilcoxon Rank Sum Test, mean + SEM bars shown.

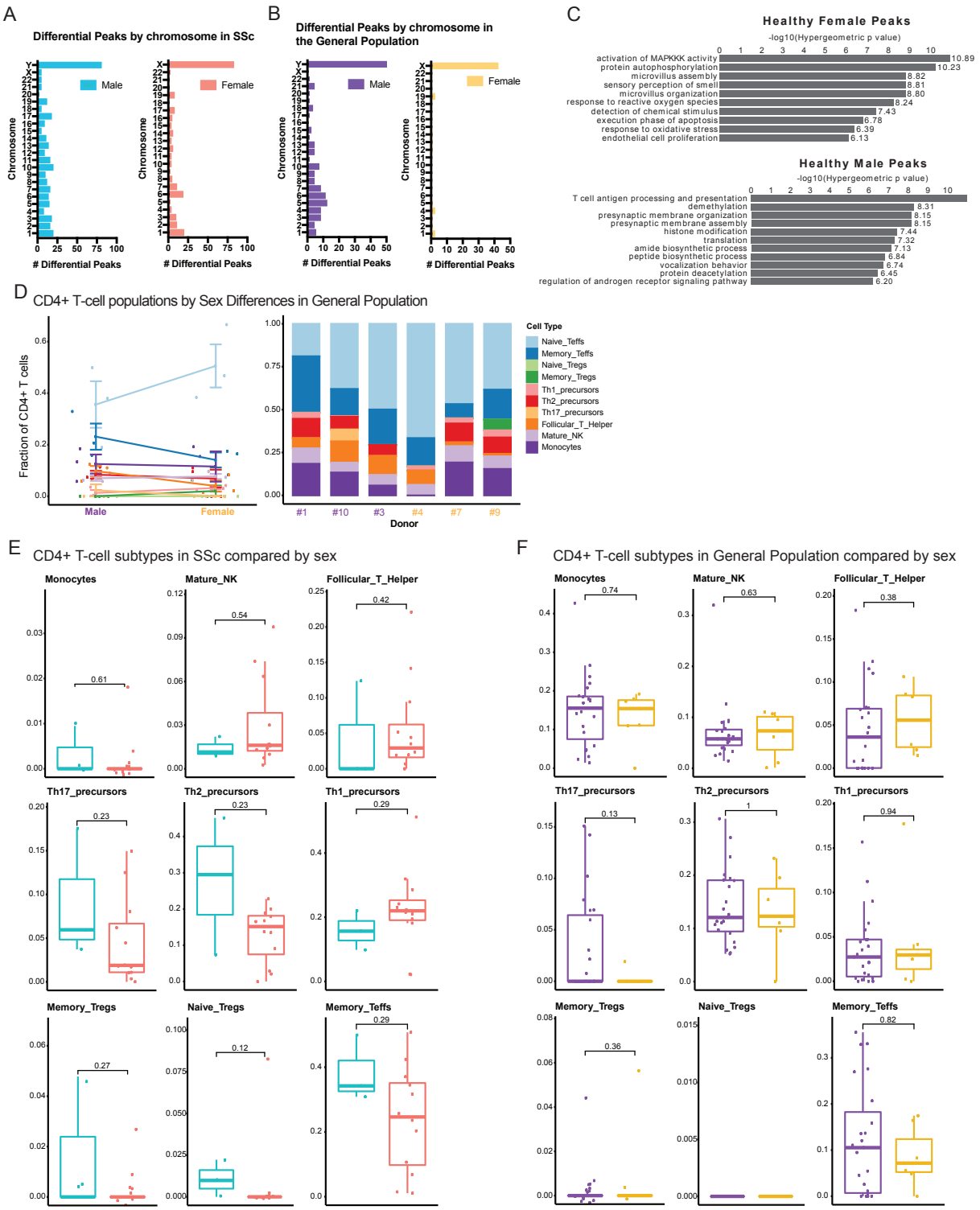

Supplemental Figure 3: *Sex-related differences in SSc study patients*. **A** Differential peaks from each chromosome grouped by sex (female = red, male = blue) in SSc study patients. **B** Differential peaks from each chromosome grouped by sex (female = yellow, male = purple) in general population healthy control samples. **C** GREAT predicted functions of cis-regulatory regions associated with peaks accessible in healthy control females and males. Statistics

calculated using Fisher's Exact test, N=3 healthy males, N=3 healthy females **D** CIBERSORT analysis of $CD4^+$ T-cell subsets in general population control males and females (composite of all patients by cell type, left, individual patient examples, right). Percentages of each $CD4^+$ T-cell subset as calculated using CIBERSORT compared by sex in **E** SSc patients (N=17, 3 timepoints each) and **F** general population controls (N=6, 3 males and 3 females). Graphs display Mean + SEM, significance calculated using the Wilcoxon Rank Sum Test

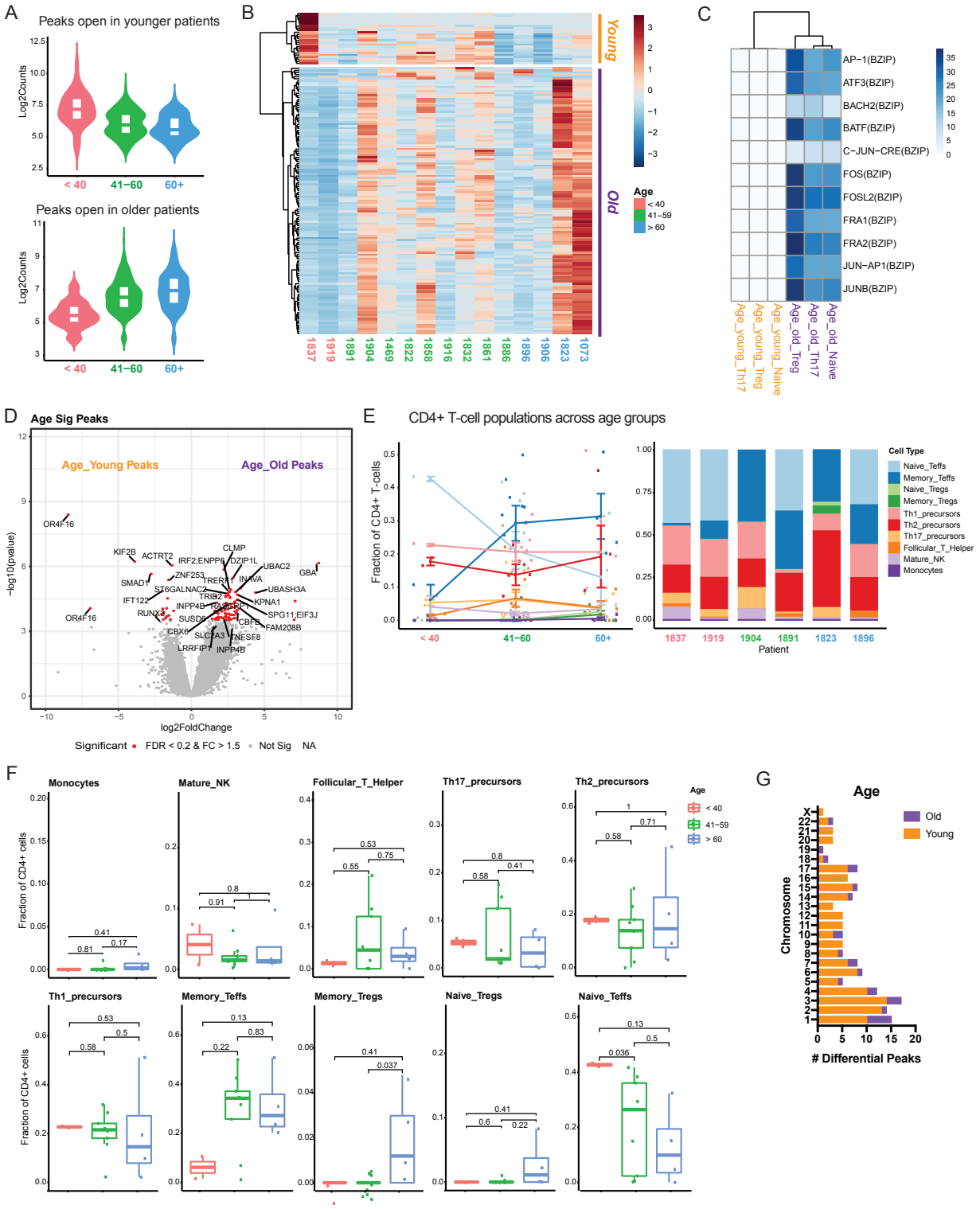

Supplemental Figure 4: *Age-related difference in SSc study patients.* **A** Violin plots depicting peaks more accessible in younger than 40 years (red), 41-60 years (green), and older than 60 years (blue) at baseline. **B** Heatmap of z-score for accessibility of differential ATAC-seq peaks of SSc study patients at treatment-naïve, baseline timepoint grouped by age (red label = younger than 40, green label = 41-60 years**,** blue label = older than 60) and clusters for peaks more

accessible in young patients (orange) and old patients (purple). **C** Heatmap of motif enrichment of the genomic region from overlay of differential ATAC-seq peaks with HiChIP anchors . **D** Volcano plot of differential peaks with FDR < 0.2 and absolute fold change larger than 1.5 highlighted in red. “Young” (orange) and “Old” (purple) refer to the two clusters from **B**. **E** CIBERSORT analysis of $CD4^+$ T-cell subsets grouped by age of SSc patients (left panel: composite of N=17 patients by cell type; right panel: individual patient examples). **F** Percentages of each $CD4^+$ T-cell subset as calculated by CIBERSORT compared by age group in SSc patients. **G** Differential peaks from each chromosome grouped by age in SSc study patients. Significance calculated using the Wilcoxon Rank Sum Test, N=18 patients across 3 timepoints each.

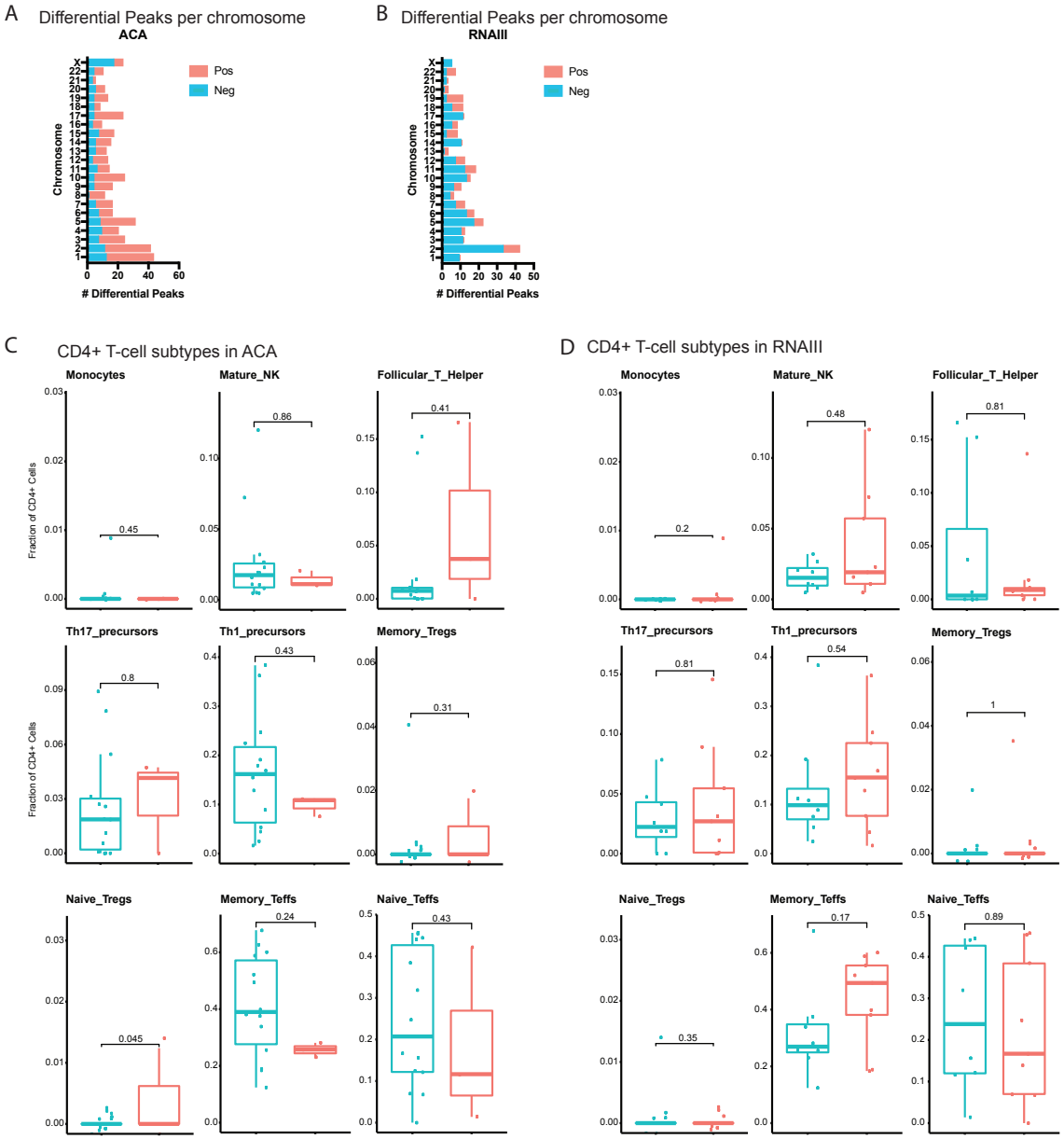

Supplemental Figure 5: *Autoantibody-related differences in SSc study patients*. Number of differential peaks at each chromosome grouped by absence and presence of **A** ACA or **B** RNAIII. Percentages of each CD4^{+} T-cell subset as calculated by CIBERSORT compared by positivity or absence of **C** ACA or **D** RNAIII in SSc study patients. Significance calculated using the Wilcoxon Rank Sum Test, N=17 patients across 3 timepoints each.

TABLES

Patient ID	Baseline Age	Sex	SSc Subtype	ACA	RNAIII	Scl70	SSc Antibodies	ANA	Treatment	Response
SScReg_ 1073	66	F	Diffuse		+		+	+	No Treatment	Stable
SScReg_ 1469	49	M	Diffuse	+			+	+	No Treatment	Worse
SScReg_ 1736	42	F	Diffuse		NA		NA	+	Other	Worse
SScReg_ 1753	33	M	Diffuse		+		+	+	MMF	Improver
SScReg_ 1759	60	F	Diffuse					+	MMF	Stable
SScReg_ 1822	43	F	Limited		+		+	+	MMF	Stable
SScReg_ 1823	61	M	Limited	+			+	+	No Treatment	Stable
SScReg_ 1832	41	F	Limited					+	MMF	Stable
SScReg_ 1837	30	F	Diffuse	NA	+		+	NA	MMF	Stable
SScReg_ 1858	48	F	Diffuse			+	+	+	No Treatment	Worse
SScReg_ 1861	47	F	Limited	+			+	+	MMF	Stable
SScReg_ 1886	58	M	Diffuse		+		+	+	MMF	Stable
SScReg_ 1891	51	F	Diffuse		+		+	+	MMF	Worse
SScReg_ 1896	63	F	Diffuse					+	MMF	Improver
SScReg_ 1904	55	F	Diffuse		+		+	+	MMF	Worse
SScReg_ 1906	70	F	Diffuse		+		+	+	Other	Stable
SScReg_ 1916	55	F	Diffuse		+		+	+	MMF	Worse
SScReg_ 1919	38	F	Diffuse					+	MMF	Worse

Table 1: *Systemic Sclerosis patient metrics involved in the study*. Metrics include the patient ID in 4 numerical digits, age at study baseline, biological sex, SSc disease subtype, anti-centromere antibody (ACA), RNA polymerase III (RNAIII) antibody, Scl70 antibody, presence of any SSc antibodies (ACA, RNAIII or Scl70), antinuclear antibody (ANA), treatment group, and response from baseline to study termination. ("+" indicates present, "NA" indicates results were not available because patient was not tested, blank indicates absence)

SUPPLEMENTAL TABLES

Supplemental Table 1: *Patient Timepoint Table.* Timepoint information (calculated in 0.5 month intervals) and baseline MRSS information for each patient.

Supplemental Table 2: *QC Table*. Quality Check metrics of ATAC-seq libraries for SSc study.

REFERENCES:

Allanore, Y., P. Wung, C. Soubrane, C. Esperet, F. Marrache, R. Bejuit, A. Lahmar, D. Khanna, C.P. Denton, and Investigators. 2020a. A randomised, double-blind, placebo-controlled, 24-week, phase II, proof-of-concept study of romilkimab (SAR156597) in early diffuse cutaneous systemic sclerosis. *Ann Rheum Dis* 79:1600-1607.

Allanore, Y., P. Wung, C. Soubrane, C. Esperet, F. Marrache, R. Bejuit, A. Lahmar, D. Khanna, C.P. Denton, and Investigators. 2020b. A randomised, double-blind, placebo-controlled, 24-week, phase II, proof-of-concept study of romilkimab (SAR156597) in early diffuse cutaneous systemic sclerosis. *Ann Rheum Dis*

Allison, A.C., and E.M. Eugui. 2000. Mycophenolate mofetil and its mechanisms of action. *Immunopharmacology* 47:85-118.

Benjamini, Y., and Y. Hochberg. 1995. Controlling the False Discovery Rate: A Practical and Powerful Approach to Multiple Testing. *Journal of the Royal Statistical Society. Series B (Methodological)* 57:289-300.

Bhattacharyya, S., V. Chandra, P. Vijayanand, and F. Ay. 2019. Identification of significant chromatin contacts from HiChIP data by FitHiChIP. *Nat Commun* 10:4221.

Brodeur, T.Y., T.E. Robidoux, J.S. Weinstein, J. Craft, S.L. Swain, and A. Marshak-Rothstein. 2015. IL-21 Promotes Pulmonary Fibrosis through the Induction of Profibrotic CD8+ T Cells. *J Immunol* 195:5251-5260.

Buenrostro, J.D., P.G. Giresi, L.C. Zaba, H.Y. Chang, and W.J. Greenleaf. 2013. Transposition of native chromatin for fast and sensitive epigenomic profiling of open chromatin, DNA-binding proteins and nucleosome position. *Nat Methods* 10:1213-1218.

Calderon, D., M.L.T. Nguyen, A. Mezger, A. Kathiria, F. Müller, V. Nguyen, N. Lescano, B. Wu, J. Trombetta, J.V. Ribado, D.A. Knowles, Z. Gao, F. Blaeschke, A.V. Parent, T.D. Burt, M.S. Anderson, L.A. Criswell, W.J. Greenleaf, A. Marson, and J.K. Pritchard. 2019. Landscape of stimulation-responsive chromatin across diverse human immune cells. *Nat Genet* 51:1494-1505.

Castelo-Branco, C., and I. Soveral. 2014. The immune system and aging: a review. *Gynecol Endocrinol* 30:16-22.

Chia, J.J., and T.T. Lu. 2015. Update on macrophages and innate immunity in scleroderma. *Curr Opin Rheumatol* 27:530-536.

Chizzolini, C., Y. Parel, C. De Luca, A. Tyndall, A. Akesson, A. Scheja, and J.M. Dayer. 2003. Systemic sclerosis Th2 cells inhibit collagen production by dermal fibroblasts via membrane-associated tumor necrosis factor alpha. *Arthritis Rheum* 48:2593-2604.

Christmann, R.B., E. Hayes, S. Pendergrass, C. Padilla, G. Farina, A.J. Affandi, M.L. Whitfield, H.W. Farber, and R. Lafyatis. 2011. Interferon and alternative activation of monocyte/macrophages in systemic sclerosis-associated pulmonary arterial hypertension. *Arthritis Rheum* 63:1718-1728.

Christmann, R.B., P. Sampaio-Barros, G. Stifano, C.L. Borges, C.R. de Carvalho, R. Kairalla, E.R. Parra, A. Spira, R. Simms, V.L. Capellozzi, and R. Lafyatis. 2014. Association of Interferon- and transforming growth factor β-regulated genes and macrophage activation with systemic sclerosis-related progressive lung fibrosis. *Arthritis Rheumatol* 66:714-725.

Clark, K.E.N., C. Campochiaro, L.V. Host, A. Sari, J. Harvey, C.P. Denton, and V.H. Ong. 2022. Combinations of scleroderma hallmark autoantibodies associate with distinct clinical phenotypes. *Scientific Reports* 12:11212.

Corces, M.R., J.D. Buenrostro, B. Wu, P.G. Greenside, S.M. Chan, J.L. Koenig, M.P. Snyder, J.K. Pritchard, A. Kundaje, W.J. Greenleaf, R. Majeti, and H.Y. Chang. 2016. Lineage-specific and single-cell chromatin accessibility charts human hematopoiesis and leukemia evolution. *Nat Genet* 48:1193-1203.

Corces, M.R., A.E. Trevino, E.G. Hamilton, P.G. Greenside, N.A. Sinnott-Armstrong, S. Vesuna, A.T. Satpathy, A.J. Rubin, K.S. Montine, B. Wu, A. Kathiria, S.W. Cho, M.R. Mumbach, A.C. Carter, M. Kasowski, L.A. Orloff, V.I. Risca, A. Kundaje, P.A. Khavari, T.J. Montine, W.J. Greenleaf, and H.Y. Chang. 2017. An improved ATAC-seq protocol reduces background and enables interrogation of frozen tissues. *Nat Methods*

Costanzo, A., M.S. Chimenti, E. Botti, R. Caruso, M. Sarra, and G. Monteleone. 2010. IL-21 in the pathogenesis and treatment of skin diseases. *J Dermatol Sci* 60:61-66.

Dantas, A.T., S.M. Gonçalves, M.C. Pereira, R.S. Gonçalves, C.D. Marques, M.J. Rego, I.a.R. Pitta, A.L. Duarte, and M.G. Pitta. 2015. Increased IL-35 serum levels in systemic sclerosis and association with pulmonary interstitial involvement. *Clin Rheumatol* 34:1621-1625.

Daoussis, D., S.N. Liossis, A.C. Tsamandas, C. Kalogeropoulou, F. Paliogianni, C. Sirinian, G. Yiannopoulos, and A.P. Andonopoulos. 2012. Effect of long-term treatment with rituximab on pulmonary function and skin fibrosis in patients with diffuse systemic sclerosis. *Clinical and experimental rheumatology* 30:S17-22.

Domsic, R.T., and T.A. Medsger. 2016. Autoantibodies and Their Role in Scleroderma Clinical Care. *Current Treatment Options in Rheumatology* 2:239-251.

Fernández-Codina, A., K.M. Walker, J.E. Pope, and S.A. Group. 2018. Treatment Algorithms for Systemic Sclerosis According to Experts. *Arthritis Rheumatol* 70:1820-1828.

Fuschiotti, P., A.T. Larregina, J. Ho, C. Feghali-Bostwick, and T.A. Medsger. 2013. Interleukin-13-producing CD8+ T cells mediate dermal fibrosis in patients with systemic sclerosis. *Arthritis Rheum* 65:236-246.

Fuschiotti, P., T.A. Medsger, and P.A. Morel. 2009. Effector CD8+ T cells in systemic sclerosis patients produce abnormally high levels of interleukin-13 associated with increased skin fibrosis. *Arthritis Rheum* 60:1119-1128.

Garrett-Sinha, L.A., A. Kearly, and A.B. Satterthwaite. 2016. The Role of the Transcription Factor Ets1 in Lupus and Other Autoimmune Diseases. *Crit Rev Immunol* 36:485-510.

Gasparini, G., E. Cozzani, and A. Parodi. 2020. Interleukin-4 and interleukin-13 as possible therapeutic targets in systemic sclerosis. *Cytokine* 125:154799.

Gjeloshi, K., G. Lettieri, F. Danzo, G. Abignano, M. Hinton, A. Dean, G. Cuomo, O. Kubassova, and F. Del Galdo. 2020. Digital Artery Volume Index (Davix©) Predicts Onset of Future Digital Ulcers in Patients with Systemic Sclerosis [abstract]. *Arthritis Rheumatol* 72:

Guilpain, P., D. Noël, and J. Avouac. 2021. Editorial: Key Players in Systemic Sclerosis: The Immune System and Beyond. *Frontiers in Immunology* 12:

Haynes, L. 2020. Aging of the Immune System: Research Challenges to Enhance the Health Span of Older Adults. *Frontiers in Aging* 1:

Heinz, S., C. Benner, N. Spann, E. Bertolino, Y.C. Lin, P. Laslo, J.X. Cheng, C. Murre, H. Singh, and C.K. Glass. 2010. Simple combinations of lineage-determining transcription factors prime

cis-regulatory elements required for macrophage and B cell identities. *Mol Cell* 38:576-589.

Herrick, A.L., M. Lunt, N. Whidby, H. Ennis, A. Silman, N. McHugh, and C.P. Denton. 2010. Observational study of treatment outcome in early diffuse cutaneous systemic sclerosis. *J Rheumatol* 37:116-124.

Higashi-Kuwata, N., M. Jinnin, T. Makino, S. Fukushima, Y. Inoue, F.C. Muchemwa, Y. Yonemura, Y. Komohara, M. Takeya, H. Mitsuya, and H. Ihn. 2010. Characterization of monocyte/macrophage subsets in the skin and peripheral blood derived from patients with systemic sclerosis. *Arthritis Res Ther* 12:R128.

Hinchcliff, M., R. Garcia-Milian, S. Di Donato, K. Dill, E. Bundschuh, and F.D. Galdo. 2021. Cellular and Molecular Diversity in Scleroderma. *Seminars in Immunology* 58:101648.

Hinchcliff, M., C.C. Huang, T.A. Wood, J. Matthew Mahoney, V. Martyanov, S. Bhattacharyya, Z. Tamaki, J. Lee, M. Carns, S. Podlusky, A. Sirajuddin, S.J. Shah, R.W. Chang, R. Lafyatis, J. Varga, and M.L. Whitfield. 2013. Molecular signatures in skin associated with clinical improvement during mycophenolate treatment in systemic sclerosis. *J Invest Dermatol* 133:1979-1989.

Hinchcliff, M., D.M. Toledo, J.N. Taroni, T.A. Wood, J.M. Franks, M.S. Ball, A. Hoffmann, S.M. Amin, A.U. Tan, K. Tom, Y. Nesbeth, J. Lee, M. Ma, K. Aren, M.A. Carns, P.A. Pioli, and M.L. Whitfield. 2018. Mycophenolate Mofetil Treatment of Systemic Sclerosis Reduces Myeloid Cell Numbers and Attenuates the Inflammatory Gene Signature in Skin. *J Invest Dermatol* 138:1301-1310.

Johnson, M.E., P.A. Pioli, and M.L. Whitfield. 2015. Gene expression profiling offers insights into the role of innate immune signaling in SSc. *Semin Immunopathol* 37:501-509.

Jordan, S., J.H. Distler, B. Maurer, D. Huscher, J.M. van Laar, Y. Allanore, O. Distler, and E.R.s. group. 2015. Effects and safety of rituximab in systemic sclerosis: an analysis from the European Scleroderma Trial and Research (EUSTAR) group. *Ann Rheum Dis* 74:1188-1194.

Kastirr, I., S. Maglie, M. Paroni, J.S. Alfen, G. Nizzoli, E. Sugliano, M.C. Crosti, M. Moro, B. Steckel, S. Steinfelder, K. Stölzel, C. Romagnani, F. Botti, F. Caprioli, M. Pagani, S. Abrignani, and J. Geginat. 2014. IL-21 is a central memory T cell-associated cytokine that inhibits the generation of pathogenic Th1/17 effector cells. *J Immunol* 193:3322-3331.

Keenan, C.R., and R.S. Allan. 2019. Epigenomic drivers of immune dysfunction in aging. *Aging Cell* 18:e12878.

Kent, W.J., A.S. Zweig, G. Barber, A.S. Hinrichs, and D. Karolchik. 2010. BigWig and BigBed: enabling browsing of large distributed datasets. *Bioinformatics* 26:2204-2207.

Khanna, D., C. Spino, S. Johnson, L. Chung, M.L. Whitfield, C.P. Denton, V. Berrocal, J. Franks, B. Mehta, J. Molitor, V.D. Steen, R. Lafyatis, R.W. Simms, A. Gill, S. Kafaja, T.M. Frech, V. Hsu, R.T. Domsic, J.E. Pope, J.K. Gordon, M.D. Mayes, E. Schiopu, A. Young, N. Sandorfi, J. Park, F.N. Hant, E.J. Bernstein, S. Chatterjee, F.V. Castelino, A. Ajam, Y. Wang, T. Wood, Y. Allanore, M. Matucci-Cerinic, O. Distler, O. Singer, E. Bush, D.A. Fox, and D.E. Furst. 2020. Abatacept in Early Diffuse Cutaneous Systemic Sclerosis: Results of a Phase II Investigator-Initiated, Multicenter, Double-Blind, Randomized, Placebo-Controlled Trial. *Arthritis Rheumatol* 72:125-136.

Kumar, R., C. Mickael, J. Chabon, L. Gebreab, A. Rutebemberwa, A.R. Garcia, D.E. Koyanagi, L. Sanders, A. Gandjeva, M.T. Kearns, L. Barthel, W.J. Janssen, T. Mauad, A. Bandeira, E.

Schmidt, R.M. Tuder, and B.B. Graham. 2015. The Causal Role of IL-4 and IL-13 in Schistosoma mansoni Pulmonary Hypertension. *Am J Respir Crit Care Med* 192:998-1008.

Langmead, B., and S.L. Salzberg. 2012. Fast gapped-read alignment with Bowtie 2. *Nat Methods* 9:357-359.

Lei, L., X.N. Zhong, Z.Y. He, C. Zhao, and X.J. Sun. 2015. IL-21 induction of CD4+ T cell differentiation into Th17 cells contributes to bleomycin-induced fibrosis in mice. *Cell Biol Int* 39:388-399.

LeRoy, E.C., C. Black, R. Fleischmajer, S. Jablonska, T. Krieg, T.A. Medsger, N. Rowell, and F. Wollheim. 1988. Scleroderma (systemic sclerosis): classification, subsets and pathogenesis. *J Rheumatol* 15:202-205.

Li, H., and R. Durbin. 2009. Fast and accurate short read alignment with Burrows-Wheeler transform. *Bioinformatics* 25:1754-1760.

Li, H., B. Handsaker, A. Wysoker, T. Fennell, J. Ruan, N. Homer, G. Marth, G. Abecasis, R. Durbin, and G.P.D.P. Subgroup. 2009. The Sequence Alignment/Map format and SAMtools. *Bioinformatics* 25:2078-2079.

Love, M.I., W. Huber, and S. Anders. 2014. Moderated estimation of fold change and dispersion for RNA-seq data with DESeq2. *Genome Biol* 15:550.

Mavalia, C., C. Scaletti, P. Romagnani, A.M. Carossino, A. Pignone, L. Emmi, C. Pupilli, G. Pizzolo, E. Maggi, and S. Romagnani. 1997. Type 2 helper T-cell predominance and high CD30 expression in systemic sclerosis. *Am J Pathol* 151:1751-1758.

McLean, C.Y., D. Bristor, M. Hiller, S.L. Clarke, B.T. Schaar, C.B. Lowe, A.M. Wenger, and G. Bejerano. 2010. GREAT improves functional interpretation of cis-regulatory regions. *Nat Biotechnol* 28:495-501.

Müller, L., S. Di Benedetto, and G. Pawelec. 2019. The Immune System and Its Dysregulation with Aging. *Subcell Biochem* 91:21-43.

Mumbach, M.R., A.T. Satpathy, E.A. Boyle, C. Dai, B.G. Gowen, S.W. Cho, M.L. Nguyen, A.J. Rubin, J.M. Granja, K.R. Kazane, Y. Wei, T. Nguyen, P.G. Greenside, M.R. Corces, J. Tycko, D.R. Simeonov, N. Suliman, R. Li, J. Xu, R.A. Flynn, A. Kundaje, P.A. Khavari, A. Marson, J.E. Corn, T. Quertermous, W.J. Greenleaf, and H.Y. Chang. 2017. Enhancer connectome in primary human cells identifies target genes of disease-associated DNA elements. *Nat Genet* 49:1602-1612.

Newman, A.M., C.L. Liu, M.R. Green, A.J. Gentles, W. Feng, Y. Xu, C.D. Hoang, M. Diehn, and A.A. Alizadeh. 2015. Robust enumeration of cell subsets from tissue expression profiles. *Nat Methods* 12:453-457.

Nguyen, B., S. Assassi, F.C. Arnett, and M.D. Mayes. 2010. Association of RNA polymerase III antibodies with scleroderma renal crisis. *J Rheumatol* 37:1068; author reply 1069.

Odler, B., V. Foris, A. Gungl, V. Müller, P.M. Hassoun, G. Kwapiszewska, H. Olschewski, and G. Kovacs. 2018. Biomarkers for Pulmonary Vascular Remodeling in Systemic Sclerosis: A Pathophysiological Approach. *Front Physiol* 9:587.

Ong, C., C. Wong, C.R. Roberts, H.S. Teh, and F.R. Jirik. 1998. Anti-IL-4 treatment prevents dermal collagen deposition in the tight-skin mouse model of scleroderma. *Eur J Immunol* 28:2619-2629.

Ong, C.J., S. Ip, S.J. Teh, C. Wong, F.R. Jirik, M.J. Grusby, and H.S. Teh. 1999. A role for T helper 2 cells in mediating skin fibrosis in tight-skin mice. *Cell Immunol* 196:60-68.

Panopoulos, S.T., V.K. Bournia, G. Trakada, I. Giavri, C. Kostopoulos, and P.P. Sfikakis. 2013. Mycophenolate versus cyclophosphamide for progressive interstitial lung disease associated with systemic sclerosis: a 2-year case control study. *Lung* 191:483-489.

Peoples, C., T.A. Medsger, M. Lucas, B.L. Rosario, and C.A. Feghali-Bostwick. 2016. Gender differences in systemic sclerosis: relationship to clinical features, serologic status and outcomes. *J Scleroderma Relat Disord* 1:177-240.

Prins, K.W., T. Thenappan, E.K. Weir, R. Kalra, M. Pritzker, and S.L. Archer. 2019. Repurposing Medications for Treatment of Pulmonary Arterial Hypertension: What's Old Is New Again. *J Am Heart Assoc* 8:e011343.

Qu, K., L.C. Zaba, P.G. Giresi, R. Li, M. Longmire, Y.H. Kim, W.J. Greenleaf, and H.Y. Chang. 2015. Individuality and variation of personal regulomes in primary human T cells. *Cell Syst* 1:51-61.

Qu, K., L.C. Zaba, A.T. Satpathy, P.G. Giresi, R. Li, Y. Jin, R. Armstrong, C. Jin, N. Schmitt, Z. Rahbar, H. Ueno, W.J. Greenleaf, Y.H. Kim, and H.Y. Chang. 2017. Chromatin Accessibility Landscape of Cutaneous T Cell Lymphoma and Dynamic Response to HDAC Inhibitors. *Cancer Cell* 32:27-41.e24.

Quinlan, A.R., and I.M. Hall. 2010. BEDTools: a flexible suite of utilities for comparing genomic features. *Bioinformatics* 26:841-842.

Raudvere, U., L. Kolberg, I. Kuzmin, T. Arak, P. Adler, H. Peterson, and J. Vilo. 2019. g:Profiler: a web server for functional enrichment analysis and conversions of gene lists (2019 update). *Nucleic Acids Res* 47:W191-W198.

Robinson, M.D., D.J. McCarthy, and G.K. Smyth. 2010. edgeR: a Bioconductor package for differential expression analysis of digital gene expression data. *Bioinformatics* 26:139-140.

Rozycki, M., M. Lodyga, J. Lam, M.Z. Miranda, K. Fátyol, P. Speight, and A. Kapus. 2014. The fate of the primary cilium during myofibroblast transition. *Mol Biol Cell* 25:643-657.

Sarra, M., R. Caruso, M.L. Cupi, I. Monteleone, C. Stolfi, E. Campione, L. Diluvio, A. Mazzotta, E. Botti, S. Chimenti, A. Costanzo, T.T. MacDonald, F. Pallone, and G. Monteleone. 2011. IL-21 promotes skin recruitment of CD4(+) cells and drives IFN-γ-dependent epidermal hyperplasia. *J Immunol* 186:5435-5442.

Saveria Fioretto, B., I. Rosa, E. Romano, Y. Wang, S. Guiducci, G. Zhang, M. Manetti, and M. Matucci-Cerinic. 2020. The contribution of epigenetics to the pathogenesis and gender dimorphism of systemic sclerosis: a comprehensive overview. *Ther Adv Musculoskelet Dis* 12:1759720X20918456.

Skaug, B., D. Khanna, W.R. Swindell, M.E. Hinchcliff, T.M. Frech, V.D. Steen, F.N. Hant, J.K. Gordon, A.A. Shah, L. Zhu, W.J. Zheng, J.L. Browning, A.M.S. Barron, M. Wu, S. Visvanathan, P. Baum, J.M. Franks, M.L. Whitfield, V.K. Shanmugam, R.T. Domsic, F.V. Castelino, E.J. Bernstein, N. Wareing, M.A. Lyons, J. Ying, J. Charles, M.D. Mayes, and S. Assassi. 2020. Global skin gene expression analysis of early diffuse cutaneous systemic sclerosis shows a prominent innate and adaptive inflammatory profile. *Ann Rheum Dis* 79:379-386.

Soon, E., A.M. Holmes, C.M. Treacy, N.J. Doughty, L. Southgate, R.D. Machado, R.C. Trembath, S. Jennings, L. Barker, P. Nicklin, C. Walker, D.C. Budd, J. Pepke-Zaba, and N.W. Morrell.

2010. Elevated levels of inflammatory cytokines predict survival in idiopathic and familial pulmonary arterial hypertension. *Circulation* 122:920-927.

Steen, V.D., M. Lucas, N. Fertig, and T.A. Medsger. 2007. Pulmonary arterial hypertension and severe pulmonary fibrosis in systemic sclerosis patients with a nucleolar antibody. *J Rheumatol* 34:2230-2235.

Sweatt, A.J., H.K. Hedlin, V. Balasubramanian, A. Hsi, L.K. Blum, W.H. Robinson, F. Haddad, P.M. Hickey, R. Condliffe, A. Lawrie, M.R. Nicolls, M. Rabinovitch, P. Khatri, and R.T. Zamanian. 2019. Discovery of Distinct Immune Phenotypes Using Machine Learning in Pulmonary Arterial Hypertension. *Circ Res* 124:904-919.

Taroni, J.N., V. Martyanov, J.M. Mahoney, and M.L. Whitfield. 2017. A Functional Genomic Meta-Analysis of Clinical Trials in Systemic Sclerosis: Toward Precision Medicine and Combination Therapy. *J Invest Dermatol* 137:1033-1041.

Teves, M.E., J.F. Strauss, P. Sapao, B. Shi, and J. Varga. 2019. The Primary Cilium: Emerging Role as a Key Player in Fibrosis. *Curr Rheumatol Rep* 21:29.

van den Hoogen, F., D. Khanna, J. Fransen, S.R. Johnson, M. Baron, A. Tyndall, M. Matucci-Cerinic, R.P. Naden, T.A. Medsger, Jr., P.E. Carreira, G. Riemekasten, P.J. Clements, C.P. Denton, O. Distler, Y. Allanore, D.E. Furst, A. Gabrielli, M.D. Mayes, J.M. van Laar, J.R. Seibold, L. Czirjak, V.D. Steen, M. Inanc, O. Kowal-Bielecka, U. Muller-Ladner, G. Valentini, D.J. Veale, M.C. Vonk, U.A. Walker, L. Chung, D.H. Collier, M.E. Csuka, B.J. Fessler, S. Guiducci, A. Herrick, V.M. Hsu, S. Jimenez, B. Kahaleh, P.A. Merkel, S. Sierakowski, R.M. Silver, R.W. Simms, J. Varga, and J.E. Pope. 2013. 2013 classification criteria for systemic sclerosis: an American College of Rheumatology/European League against Rheumatism collaborative initiative. *Arthritis Rheum* 65:2737-2747.

Walker, K.M., J. Pope, p.m.o.t.S.C.T.C. (SCTC), and C.S.R.G. (CSRG). 2012. Treatment of systemic sclerosis complications: what to use when first-line treatment fails--a consensus of systemic sclerosis experts. *Semin Arthritis Rheum* 42:42-55.

Wurster, A.L., V.L. Rodgers, A.R. Satoskar, M.J. Whitters, D.A. Young, M. Collins, and M.J. Grusby. 2002. Interleukin 21 is a T helper (Th) cell 2 cytokine that specifically inhibits the differentiation of naive Th cells into interferon gamma-producing Th1 cells. *J Exp Med* 196:969-977.

Xu, J., K. Nuno, U.M. Litzenburger, Y. Qi, M.R. Corces, R. Majeti, and H.Y. Chang. 2019. Single-cell lineage tracing by endogenous mutations enriched in transposase accessible mitochondrial DNA. *Elife* 8:

Zamanian, R., D. Badesch, L. Chung, R. Domsic, T. Medsger, A. Pinckney, L. Keyes-Elstein, C. D'Aveta, M. Spychala, J. White, P. Hassoun, F. Torres, J. Molitor, D. Khanna, H. Maeker, B. Welch, E. Goldmuntz, M. Nicolls, and -. On Behalf Of Asco1 Investigators. 2019. Late Breaking Abstract - Safety and efficacy of B-cell depletion with rituximab for the treatment of systemic sclerosis-associated pulmonary arterial hypertension. *European Respiratory Journal* 54:RCT1884.

Zamanian, R.T., D. Badesch, L. Chung, R.T. Domsic, T. Medsger, A. Pinckney, L. Keyes-Elstein, C. D'Aveta, M. Spychala, R.J. White, P.M. Hassoun, F. Torres, A.J. Sweatt, J.A. Molitor, D. Khanna, H. Maecker, B. Welch, E. Goldmuntz, and M.R. Nicolls. 2021. Safety and Efficacy of B-Cell Depletion with Rituximab for the Treatment of Systemic Sclerosis-associated

Pulmonary Arterial Hypertension: A Multicenter, Double-Blind, Randomized, Placebo-controlled Trial. *Am J Respir Crit Care Med* 204:209-221.

Zhang, Y., T. Liu, C.A. Meyer, J. Eeckhoute, D.S. Johnson, B.E. Bernstein, C. Nusbaum, R.M. Myers, M. Brown, W. Li, and X.S. Liu. 2008. Model-based analysis of ChIP-Seq (MACS). *Genome Biol* 9:R137.